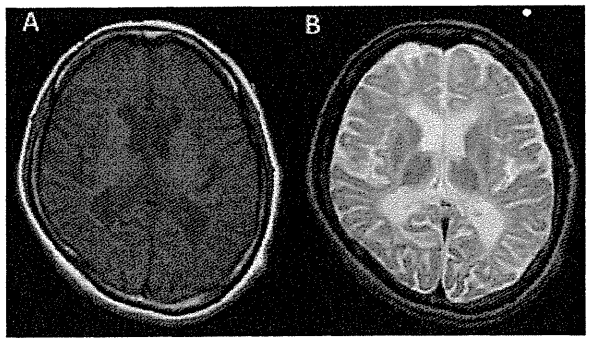

FIGURE 1: Magnetic resonance imaging of the cerebrum. (A) T1-weighted image of the proband at 20 years shows cerebral atrophy with ventricular dilatation and widening of a subarachnoidal space. Disappearance of contrast between cortex and white matter, which suggested incomplete myelination throughout the cerebrum, was evident. (B) T2-weighted image reveals diffuse hyperintensity in the white matter, suggesting the arrest of myelination. Note that the inner capsule, which is usually myelinated in the neonate, was not myelinated in this patient.

mal. Molecular examinations excluded *PLP1* exonic mutations, large duplications, and deletions.

Informed consent was obtained from the patient and family members in accordance with human study protocols approved by the institutional review board of Kanagawa Children's Medical Center. Genomic DNA was extracted from peripheral lymphocytes. A genome-wide single nucleotide polymorphism (SNP) genotyping was undertaken for III-1, III-3, IV-1, IV-2, V-1, and V-2 (Fig 2A) using the GeneChip Human Mapping 10K Array *Xba* 142 2.0 (Affymetrix, Santa Clara, CA) containing 10,204 SNPs according to the manufacture's protocols (Supplementary Materials and Methods). Polymerase chain reaction and DNA sequencing are described in the Supplementary Materials and Methods (Supplementary Table 1).

Mammalian cell expression plasmids for the wild-type and E189X mutant human *SOX10* cDNA were reported previously.[12] Luciferase reporter plasmids containing mouse *Gjc2* promoters (kindly provided from Dr M. Wegner) were utilized

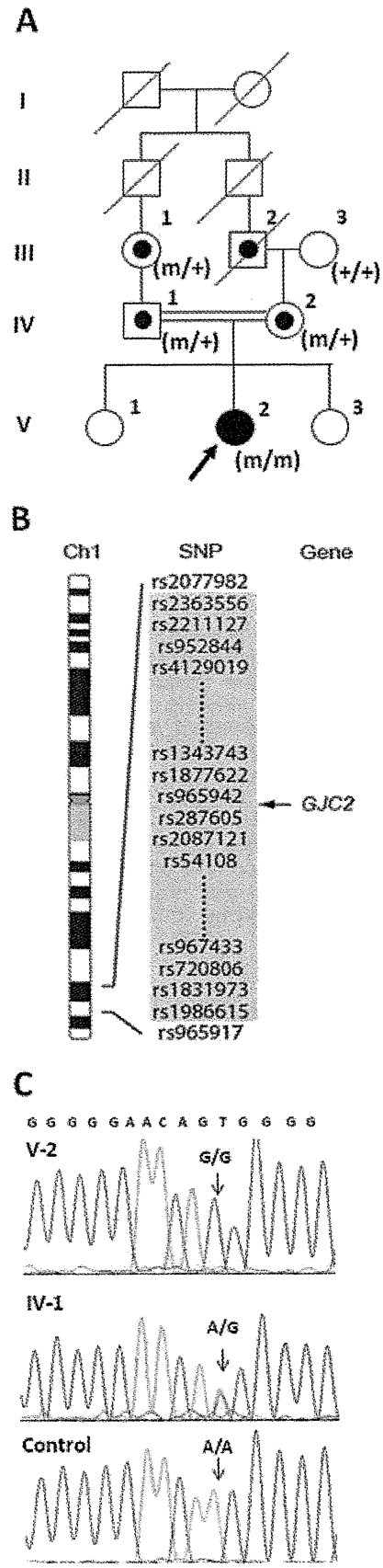

FIGURE 2: Family pedigree, largest region of interest on chromosome 1, and the *CJC2* mutation. (A) Pedigree of the Pelizaeus-Merzbacher-like disease family with the proband *(filled circle with arrow)*. DNA from III-1, III-3, IV-1, IV-2, V-1, and V-2 were used for single nucleotide polymorphism (SNP) genotyping. Carriers are indicated as circles with black dots. m = mutant allele; + = wild-type allele. (B) The largest region of interest by homozygosity SNP mapping at 1q41-q42.2. The homozygous interval is shown as a shaded square with SNP identifiers. The location of *GJC2* is shown with an arrow. The region between rs2077982 and rs965917 was 18.2 Mb in size (University of California, Santa Cruz genome browser coordinate, chromosome 1: 215150317-233384165, February 2009 version). (C) Sequencing chromatograms from the patient (V-2, top), a carrier (IV-1, middle), and a normal control (bottom). The c.-167A>G mutation in the promoter region of *CJC2* is shown with arrows.

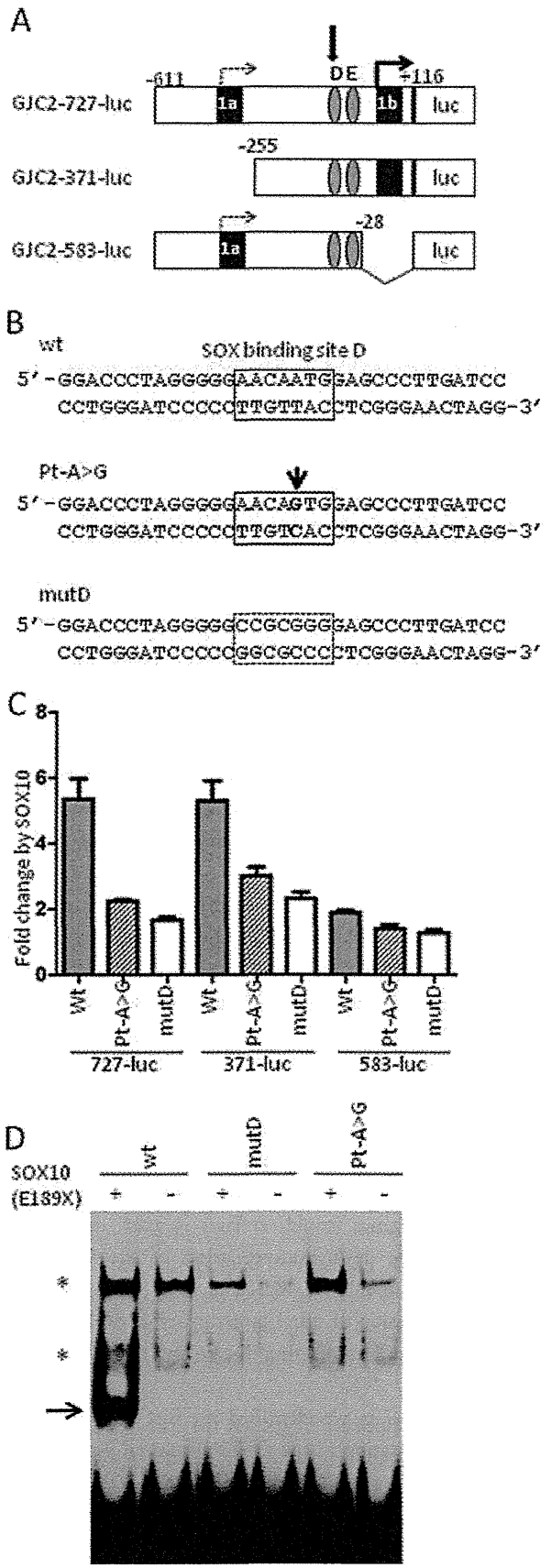

for site-directed mutagenesis (see Supplementary Materials and Methods). We measured *GJC2* transcriptional activity by luciferase reporter assays using human glioblastoma U138 cells (see Supplementary Materials and Methods). SOX10 binding affinity was determined by electrophoretic mobility shift assay (EMSA) using synthetic oligonucleotide probes and nuclear extracts from HeLa cells transfected with pCMV-SOX10-E189X, as previously described.[13]

Results

The largest region with homozygosity identified by SNP genotyping on chromosome 1q42.13 was our primary focus for candidate gene scanning (see Fig 2B, Supplementary Table 2, Supplementary Fig 1). Among 115 refseq genes mapped within this region, 34 gene products were identified from mouse whole brain proteomics studies (Supplementary Table 3).[14,15] After we sequenced all coding regions and intron-exon boundaries of these 34 genes to exclude any disease-causing mutations, we extended our analysis to promoter regions. We found a homozygous mutation, c.-167A>G, in the proximal promoter re-

FIGURE 3: Functional consequence of the c.-167A>G point mutation in the *GJC2* promoter. (A) Schematic diagram of the luciferase reporter constructs of mouse *Gjc2* promoter region utilized in this study. Exon 1b contains the major transcription start site *(thick arrow)*, whereas exon 1a contains the minor site *(dotted arrow)*. GJC2-727-luc contains a full proximal promoter, whereas GJC2-371-luc lacks exon 1a and the upstream portion and GJC2-583-luc lacks exon 1b. Two SOX10 binding site, D and E, are shown as shaded ovals with a thick arrow pointing to site D, where the mutation was identified. (B) Sequences of the probes used for electrophoretic mobility shift assays (EMSAs). Top: *wt* probe containing the wild-type site D *(square)*. Middle: Pt-A>G probe carrying c.-167A>G mutation *(arrow)*. Bottom: mutD probe in which site D was changed to abolish SOX10 binding. (C) Transcriptional activities of different *GJC2* promoter constructs carrying either wt, Pt-A>G, or mutD at site D shown as fold changes obtained by presence or absence of SOX10 determined by luciferase reporter assay. Note that the *wt* constructs for 727-luc and 371-luc, harboring the major start site in exon 1b, were activated by SOX10 >5-fold. In contrast, a much smaller effect was observed when either Pt-A>G or mutD was introduced. The 583-luc constructs, which only harbor a minor transcription start site, remain inactivated by SOX10 regardless of changes in site D. Each bar represents average ± standard deviation. Each experiment was performed 3×, each in triplicate. Results from a representative experiment were shown. (D) DNA binding affinity of each probe (shown in B) was determined by EMSA using nuclear extracts from HeLa cells transfected with plasmid expressing truncated SOX10 protein (E189X) or empty plasmid (as a negative control). The wt probe showed a strong binding to E189X SOX10 protein, which retains enhanced DNA binding ability *(arrow)*. In contrast, we observed no binding of the mutant probes, either mutD or Pt-A>G. Asterisks show nonspecific binding. Free probes were observed at the bottom of the picture.

gion of *GJC2* that segregated with PMLD in the family members (see Fig 2A and C) and was absent in 122 normal Japanese chromosomes. Analysis of this region in 10 additional female PMLD patients without mutations in the open reading frame of *GJC2* detected no abnormalities.

Interestingly, this mutation is located within a critical SOX10 binding site (designated as site D) in the syntenic mouse *Gjc2* proximal promoter and diminishes the consensus of the SOX binding sequence (AACAATG to AACAGTG, Fig 3A and B). Based on this, we predicted that this mutation disrupts *GJC2* promoter activity and measured transcription in vitro using a luciferase reporter system. Because the region harboring the mutation is highly conserved across mammals,[16] we introduced this mutation into well-studied mouse *Gjc2* promoter constructs (see Fig 3A and B). The c.-167A>G point mutation in the SOX10 binding site dramatically decreased transcription to levels similar to a completely disrupted SOX10 binding site D (see Fig 3C). These findings suggest that the c.-167A>G point mutation found in our patients results in a diminished *GJC2* transcription.

Based on these results, we hypothesized that this mutation altered SOX10 binding affinity to site D and tested this by EMSA. Because full-length SOX10 has a low binding affinity that is difficult to distinguish from background noise, we used a C-terminus truncation version of SOX10, E189X, which retains the HMG binding domain and has enhanced binding affinity.[16] Introduction of the c.-167A>G mutation into site D resulted in a complete loss of E189X SOX10 binding (see Fig 3D). Therefore, combined with the preceding observations, we find that the c.-167A>G mutation abolishes SOX10 binding to the *GJC2* promoter, resulting in a dramatic attenuation of the *GJC2* transcription.

Discussion

GJC2 encodes Cx47, a member of the connexin family. Connexins are components of gap junctions, intercellular channels that allow ions and small molecules to pass across neighboring plasma membranes. Gap junctions have diverse functions, including the propagation of electrical signals and metabolic cooperation. Two hemichannels, each built up of 6 connexin protein subunits on opposing cell membranes, form the channel. Astrocytes and oligodendrocytes are coupled by gap junctions constructed predominantly of GJC2 (Cx47) and Cx43.[17] Because Cx47 proteins carrying PMLD-causing mutations either fail to reach the membrane or have reduced transport activity, loss of function is likely the mechanism underlying the CNS hypomyelination in PMLD.[7,9] Herein we report the first *GJC2* promoter mutation,[18] c.-167A>G, in a patient with PMLD, and this is associated with allelic transcription failure.

Our female patient had nystagmus, spasticity, and choreoathetosis, clinical symptoms common to PMD and PMDL. However, she attained normal motor and intellectual developmental milestones. Because only $\frac{1}{3}$ (11 of 33) of PMLD patients with *GJC2* mutations have walked unsupported,[2–7] her clinical manifestation was mild and overlaps with that of spastic paraplegia phenotype. Of note, she lost her motor and cognitive abilities within a few years, accompanied by progressive brain atrophy (see Fig 1). Such acute regression has rarely been observed in PMD and is more characteristic of PMLD secondary to *GJC2* mutations.[6]

A recent study showed that SOX10 directly regulates *GJC2* by binding to its proximal promoter.[16] Site D, the SOX10 binding site in which our mutation was identified, plays a predominant role in *GJC2* promoter activity,[16] and the c.-167A>G mutation we identified reduces its affinity for SOX10 and abolishes *GJC2* transcription. These findings suggest that *SOX10* regulation of *GJC2* via site D is essential for proper *GJC2* expression and that its failure causes PMLD. Presumably, the relatively milder clinical phenotype observed in our patient results from reduced but not completely abolished transcriptional activity, allowing translation of a small amount of normal Cx47 protein.

This constitutes the second disorder associated with dysregulation of a SOX10 target gene. Previously, mutations within the *SOX10* binding site of the *GJB1* promoter have been shown to cause demyelinating peripheral neuropathy.

Together the peripheral neuropathy and PMLD provide a partial understanding of the clinical manifestations of PCWH patients. Because these patients have SOX10 mutations,[10] we predict that the expression of both *GJC2* and *GJB1* is impaired. Impaired expression of both of these genes would, at least in part, respectively account for the de-/hypomyelination of the CNS and PNS observed in PCWH. Based on this, we predict that impaired expression of other target genes of SOX10 is responsible for the Hirschprung disease and other Waardenburg features.

In conclusion, we identified the first case of PMLD caused by a mutation in the *GJC2* promoter. Because this mutation disrupts SOX10 regulation of *GJC2* transcription, we hypothesize that SOX10 regulation of transcription plays a major role in nervous system myelination.

Acknowledgments

This study was supported by grants-in-aid for scientific research from the Ministry of Education, Culture, Sports, Science, and Technology, Japan (H.O., K.I.), Takeda Science Foundation (H.O.), Yokohama Foundation for Advancement of Medical Science (H.O.), and Kanagawa children's hospital (K.K., H.O.), and Health Labor Sciences Research Grants from the Ministry of Health, Labor, and Welfare, Japan (H.O., K.K., N.M., K.I.).

We thank Dr M. Wegner for kindly providing us plasmid DNAs and Drs C. Boerkoel, C. du Souich, and P. Atkins for their critical reviews.

Potential Conflicts of Interest

Nothing to report.

References

1. Inoue K. PLP1-related inherited dysmyelinating disorders: Pelizaeus-Merzbacher disease and spastic paraplegia type 2. Neurogenetics 2005;6:1–16.
2. Uhlenberg B, Schuelke M, Ruschendorf F et al. Mutations in the gene encoding gap junction protein alpha 12 (connexin 46.6) cause Pelizaeus-Merzbacher-like disease. Am J Hum Genet. 2004;75:251–260.
3. Bugiani M, Al Shahwan S, Lamantea E et al. GJA12 mutations in children with recessive hypomyelinating leukoencephalopathy. Neurology. 2006;67:273-279.
4. Wolf NI, Cundall M, Rutland P et al. Frameshift mutation in GJA12 leading to nystagmus, spastic ataxia and CNS dys-/demyelination. Neurogenetics. 2007;8:39–44.
5. Salviati L, Trevisson E, Baldoin MC et al. A novel deletion in the GJA12 gene causes Pelizaeus-Merzbacher-like disease. Neurogenetics. 2007;8:57-60.
6. Henneke M, Combes P, Diekmann S et al. GJA12 mutations are a rare cause of Pelizaeus-Merzbacher-like disease. Neurology. 2008;70:748-754.
7. Orthmann-Murphy JL, Salsano E, Abrams CK et al. Hereditary spastic paraplegia is a novel phenotype for GJA12/GJC2 mutations. Brain. 2009;132:426–438.
8. Wang J, Wang H, Wang Y et al. Two novel gap junction protein alpha 12 gene mutations in two Chinese patients with Pelizaeus-Merzbacher-like disease. Brain Dev. 2009; doi:10.1016/j.braindev.2009.03.013.
9. Orthmann-Murphy JL, Enriquez AD, Abrams CK, Scherer SS. Loss-of-function GJA12/Connexin47 mutations cause Pelizaeus-Merzbacher-like disease. Mol Cell Neurosci. 2007;34:629–641.
10. Pingault V, Bondurand N, Kuhlbrodt K et al. SOX10 mutations in patients with Waardenburg-Hirschsprung disease. Nat Genet. 1998;18:171-173.
11. Nezu A, Kimura S, Uehara S et al. Pelizaeus-Merzbacher-like disease: female case report. Brain Dev. 1996;18:114–118.
12. Inoue K, Khajavi M, Ohyama T et al. Molecular mechanisms for distinct neurological phenotypes conveyed by allelic truncating mutations. Nat Genet. 2004;36:361–369.
13. Inoue K, Ohyama T, Sakuragi Y et al. Translation of SOX10 3' untranslated region causes a complex severe neurocristopathy by generation of a deleterious functional domain. Hum Mol Genet. 2007;16:3037–3046.
14. Taylor CM, Marta CB, Claycomb RJ et al. Proteomic mapping provides powerful insights into functional myelin biology. Proc Natl Acad Sci U S A. 2004;101:4643–4648.
15. Wang H, Qian WJ, Chin MH et al. Characterization of the mouse brain proteome using global proteomic analysis complemented with cysteinyl-peptide enrichment. J Proteome Res. 2006;5:361–369.
16. Schlierf B, Werner T, Glaser G, Wegner M. Expression of connexin47 in oligodendrocytes in regulated by the Sox10 transcription factor. J Mol Biol. 2006;361:11–21.
17. Orthmann-Murphy JL, Freidin M, Fischer E et al. Two distinct heterotypic channels mediate gap junction coupling between astrocyte and oligodendrocyte connexins. J Neurosci. 2007;27:13949–13957.
18. Ruf N, Uhlenberg B. Analysis of human alternative first exons and copy number variation of the GJA12 gene in patients with Pelizaeus-Merzbacher-like disease. Am J Med Genet B Neuropsychiatr Genet. 2009;150B:226–232.
19. Bondurand N, Girard M, Pingault V et al. Human Connexin 32, a gap junction protein altered in the X-linked form of Charcot-Marie-Tooth disease, is directly regulated by the transcription factor SOX10. Hum Mol Genet. 2001;10:2783-2795.
20. Houlden H, Girard M, Cockerell C et al. Connexin 32 promoter P2 mutations: a mechanism of peripheral nerve dysfunction. Ann Neurol. 2004;56:730–734.

nature genetics

Exome sequencing identifies *MLL2* mutations as a cause of Kabuki syndrome

Sarah B Ng[1,7], Abigail W Bigham[2,7], Kati J Buckingham[2], Mark C Hannibal[2,3], Margaret J McMillin[2], Heidi I Gildersleeve[2], Anita E Beck[2,3], Holly K Tabor[2,3], Gregory M Cooper[1], Heather C Mefford[2], Choli Lee[1], Emily H Turner[1], Joshua D Smith[1], Mark J Rieder[1], Koh-ichiro Yoshiura[4], Naomichi Matsumoto[5], Tohru Ohta[6], Norio Niikawa[6], Deborah A Nickerson[1], Michael J Bamshad[1–3] & Jay Shendure[1]

We demonstrate the successful application of exome sequencing[1–3] to discover a gene for an autosomal dominant disorder, Kabuki syndrome (OMIM%147920). We subjected the exomes of ten unrelated probands to massively parallel sequencing. After filtering against existing SNP databases, there was no compelling candidate gene containing previously unknown variants in all affected individuals. Less stringent filtering criteria allowed for the presence of modest genetic heterogeneity or missing data but also identified multiple candidate genes. However, genotypic and phenotypic stratification highlighted *MLL2*, which encodes a Trithorax-group histone methyltransferase[4]: seven probands had newly identified nonsense or frameshift mutations in this gene. Follow-up Sanger sequencing detected *MLL2* mutations in two of the three remaining individuals with Kabuki syndrome (cases) and in 26 of 43 additional cases. In families where parental DNA was available, the mutation was confirmed to be *de novo* ($n = 12$) or transmitted ($n = 2$) in concordance with phenotype. Our results strongly suggest that mutations in *MLL2* are a major cause of Kabuki syndrome.

Kabuki syndrome is a rare, multiple malformation disorder characterized by a distinctive facial appearance (**Supplementary Fig. 1**), cardiac anomalies, skeletal abnormalities, immunological defects and mild to moderate mental retardation. Originally described in 1981 (refs. 5,6), Kabuki syndrome has an estimated incidence of 1 in 32,000 (ref. 7), and approximately 400 cases have been reported worldwide. The vast majority of reported cases have been sporadic, but parent-to-child transmission in more than a half dozen instances[8] suggests that Kabuki syndrome is an autosomal dominant disorder. The relatively low number of cases, the lack of multiplex families and the phenotypic variability of Kabuki syndrome have made the identification of the gene(s) underlying this disorder intractable to conventional approaches of gene discovery, despite aggressive efforts.

We sequenced the exomes of ten unrelated individuals with Kabuki syndrome: seven of European ancestry, two of Hispanic ancestry and one of mixed European and Haitian ancestry (**Supplementary Fig. 1** and **Supplementary Table 1**). Enrichment was performed by hybridization of shotgun fragment libraries to custom microarrays followed by massively parallel sequencing[1–3]. On average, 6.3 gigabases of sequence were generated per sample to achieve 40× coverage of the mappable, targeted exome (31 Mb). As with our previous studies, we focused our analyses here primarily on nonsynonymous variants, splice acceptor and donor site mutations and coding indels, anticipating that synonymous variants were far less likely to be pathogenic. We also predicted that variants underlying Kabuki syndrome are rare, and therefore likely to be previously unidentified. We defined variants as previously unidentified if they were absent from all datasets used for comparison, including dbSNP129, the 1000 Genomes Project, exome data from 16 individuals previously reported by us[2,3] and 10 exomes sequenced as part of the Environmental Genome Project (EGP).

Under a dominant model in which each case was required to have at least one previously unidentified nonsynonymous variant, splice acceptor and donor site mutation or coding indel variant in the same gene, only a single candidate gene (*MUC16*) was shared across all ten exomes (**Table 1** and **Supplementary Table 2**). However, we considered *MUC16* as a likely false positive due to its extremely large size (14,507 amino acids). Potential explanations for our failure to find a compelling candidate gene in which newly identified variants were seen in all affected individuals included: (i) Kabuki syndrome is genetically heterogeneous and therefore not all affected individuals will have mutations in the same gene; (ii) we failed to identify all mutations in the targeted exome; and (iii) some or all causative mutations were outside of the targeted exome, for example, in noncoding regions or unannotated genes. To allow for a modest degree of genetic heterogeneity and/or missing data, we conducted a less stringent analysis by looking for candidate genes shared among subsets of affected individuals. Specifically, we searched

[1]Department of Genome Sciences, University of Washington, Seattle, Washington, USA. [2]Department of Pediatrics, University of Washington, Seattle, Washington, USA. [3]Seattle Children's Hospital, Seattle, Washington, USA. [4]Department of Human Genetics, Nagasaki University Graduate School of Biomedical Sciences, Nagasaki, Japan. [5]Department of Human Genetics, Yokohama City University Graduate School of Medicine, Yokohama, Japan. [6]Research Institute of Personalized Health Sciences, Health Sciences University of Hokkaido, Hokkaido, Japan. [7]These authors contributed equally to this work. Correspondence should be addressed to J.S. (shendure@u.washington.edu) or M.J.B. (mbamshad@u.washington.edu).

Received 28 April; accepted 21 July; published online 15 August 2010; doi:10.1038/ng.646

Table 1 Number of genes common to any subset of *x* affected individuals.

Subset analysis (any *x* of 10)	1	2	3	4	5	6	7	8	9	10
NS/SS/I	12,042	8,722	7,084	6,049	5,289	4,581	3,940	3,244	2,486	1,459
Not in dbSNP129 or 1000 Genomes	7,419	2,697	1,057	488	288	192	128	88	60	34
Not in control exomes	7,827	2,865	1,025	399	184	90	50	22	7	2
Not in either	6,935	2,227	701	242	104	44	16	6	3	1
Is loss-of-function (nonsense or frameshift indel)	753	49	7	3	2	2	1	0	0	0

The number of genes with at least one nonsynonymous variant (NS), splice-site acceptor or donor variants (SS) or coding indel (I) are listed under various filters. Variants were filtered by presence in dbSNP or 1000 Genomes (not in dbSNP129 or 1000 genomes) and control exomes (not in control exomes) or both (not in either); control exomes refer to those from 8 Hapmap[3], 4 FSS[3], 4 Miller[2] and 10 EGP samples. The number of genes found using the union of the intersection of *x* individuals is given.

for subsets of *x* out of 10 exomes having ≥1 previously unidentified variant in the same gene, with $x = 1$ to $x = 10$. For $x = 9$, $x = 8$ and $x = 7$, previously unidentified variants were shared in 3 genes, 6 genes and 16 genes, respectively (**Table 1**). However, there was no obvious way to rank these candidate genes.

We speculated that genotypic and/or phenotypic stratification would facilitate the prioritization of candidate genes identified by subset analysis. Specifically, we assigned a categorical rank to each individual with Kabuki syndrome based on a subjective assessment of the presence of, or similarity to, the canonical facial characteristics of Kabuki syndrome (**Supplementary Fig. 1**) and the presence of developmental delay and/or major birth defects (**Supplementary Table 1**). The highest-ranked individual was one of a pair of monozygotic twins with Kabuki syndrome. We then categorized the functional impact (that is, nonsense versus nonsynonymous substitution, splice-site disruption and frameshift compared to in-frame indel) of each newly identified variant in candidate genes shared by each subset of two or more ranked cases. Manual review of these data highlighted distinct, previously unidentified nonsense variants in *MLL2* in each of the four highest-ranked cases. After sequential analysis of phenotype-ranked cases with a loss-of-function filter, *MLL2* was the only candidate gene remaining after addition of the second individual (**Table 2**). We found no such variant in *MLL2* in the individual with Kabuki syndrome ranked fifth; hence, the number of candidate genes dropped to zero after the individual ranked fourth in the set (**Table 2**). However, we found a 4-bp deletion in the individual ranked sixth, and we found nonsense variants in the individuals ranked seventh and ninth. Thus, exome sequencing identified a nonsense substitution or frameshift indel in *MLL2* in seven of the ten individuals with Kabuki syndrome analyzed here.

Retrospectively, we applied a loss-of-function filter to the subset analysis of exome data (**Table 1**), and at $x = 7$, found *MLL2* to be the only candidate gene. We also developed a *post hoc* ranking of candidate genes based on the functional impact of the variants present (variant score) and the rank of the cases in which each variant was observed (case score). When this was applied to the exome data as a combined metric, *MLL2* emerged as the top candidate gene (**Supplementary Fig. 2**).

In parallel with these analyses, we applied genomic evolutionary rate profiling (GERP)[9] to the exome data. GERP uses mammalian genome alignments to define a rejected substitution score for each variant regardless of functional class. We have previously shown that the quantitative ranking of candidate genes by the rejected substitution scores of their variants can facilitate the exome-based analysis of Mendelian disorders[10]. Following subset analysis with GERP-based ranking, *MLL2* remained on the candidate list up to $x = 8$, ranking third in a list of 11 candidate genes at this threshold (**Table 3** and **Supplementary Fig. 3**). Notably, the additional *MLL2* variant contributing to this analysis (such that *MLL2* was still considered at $x = 8$) was a synonymous substitution with a rejected substitution score of 0.368 in the individual ranked fifth.

We sought to confirm all newly identified variants in *MLL2*, particularly because loss-of-function variants identified through massively parallel sequencing have a high prior probability of being false positives. All seven loss-of-function variants in *MLL2* were validated by Sanger sequencing. We further analyzed the three cases in which we did not initially find a loss-of-function variant in *MLL2*, first by array comparative genomic hybridization (aCGH) to determine any gross structural changes and then by Sanger sequencing of all exons of *MLL2* in case of false negatives by exome sequencing. Because an average of 96% of the coding bases in *MLL2* were called at sufficient quality and coverage for single nucleotide variant detection, we anticipated that any missed variants were more likely to be indels because of the higher coverage required for confident indel detection in short-read sequence data. Indeed, although aCGH did not find any structural variants in the region, Sanger sequencing did identify frameshift indels in two of these three cases (specifically, the cases ranked eighth and tenth).

Ultimately, loss-of-function mutations in *MLL2* were identified in nine out of ten cases in the discovery cohort (**Fig. 1**), making this gene a compelling candidate for Kabuki syndrome. For validation, we screened all 54 exons of *MLL2* in 43 additional cases by Sanger sequencing. Previously unidentified nonsynonymous, nonsense or frameshift mutations in *MLL2* were found in 26 of these 43 cases (**Fig. 1** and **Supplementary Table 3**). In total, through either exome sequencing or targeted sequencing of *MLL2*, 33 distinct *MLL2* mutations were identified in 35 of 53 families (66%) with Kabuki syndrome (**Fig. 1** and **Supplementary Table 3**). In each of 12 cases for which DNA from both parents was available, the *MLL2* variant was found to have occurred *de novo*. Three mutations were found in two individuals each. One of these three mutations was confirmed to have arisen *de novo* in one of the cases, indicating that some mutations in individuals with Kabuki syndrome are recurrent. In addition, *MLL2* mutations (resulting in p.4527K>X and p.5464T>M) were also identified in each of two families in which Kabuki syndrome was transmitted from parent to child.

Table 2 Number of genes common in sequential analysis of phenotypically ranked individuals

Sequential analysis	1	+2	+3	+4	+5	+6	+7	+8	+9	+10
NS/SS/I	5,282	3,850	3,250	2,354	2,028	1,899	1,772	1,686	1,600	1,459
Not in dbSNP129 or 1000 Genomes	687	214	145	84	63	54	42	40	39	34
Not in control exomes	675	134	50	26	13	13	8	5	4	2
Not in either	467	89	34	18	9	8	4	4	3	1
Is loss-of-function (nonsense/frameshift indel)	25	1	1	1	0	0	0	0	0	0

Variants were filtered as in **Table 1**. Exomes were added sequentially to the analysis by ranked phenotype; for example, column "+3" shows the number of genes at the intersection of the three top ranked cases (**Supplementary Fig. 1**). The gene with at least one NS/SS/I in all individuals is *MUC16*, which is very likely to be a false positive due to its extreme length (14,507 amino acids).

Table 3 Analysis of exome variants using genomic evolutionary rate profiling

GERP score analysis (at least *x* of 10)	1	2	3	4	5	6	7	8	9	10
Variant RS score > 0	7,176	2,360	754	269	106	39	20	11	3	1
MLL2 rank	3,732	1,232	399	136	47	14	6	3	NA	NA

The number of genes with at least a single previously unidentified variant with a rejected substitution score[10] > 0 in at least *x* individuals is given. A gene rank is assigned based on the average GERP score[9] over all newly identified variants with rejected substitution score > 0 in all affected individuals.

None of the additional *MLL2* mutations was found in 190 control chromosomes from individuals of matched geographical ancestry.

Our results strongly suggest that mutations in *MLL2* are a major cause of Kabuki syndrome. *MLL2* encodes a large 5,262-residue protein that is part of the SET family of proteins, of which Trithorax, the *Drosophila* homolog of MLL, is the best characterized[11]. The SET domain of MLL2 confers strong histone 3 lysine 4 methyltransferase activity and is important in the epigenetic control of active chromatin states[12]. In mice, loss of *Mll2* on a mixed 129Sv/C57BL/6 background slows growth, increases apoptosis and retards development, leading to early embryonic lethality due in part to misregulation of homeobox gene expression[13]. However, no morphological defects have been reported in $Mll2^{+/-}$ mice[13].

Most of the *MLL2* variants identified in individuals with Kabuki syndrome are predicted to truncate the polypeptide chain before translation of the SET domain. Though it is not certain whether Kabuki syndrome results from haploinsufficiency or from a gain of function at *MLL2*, haploinsufficiency seems to be the more likely mechanism. Deletion of chromosome 12q12–q13.2, which encompasses *MLL2*, has been reported in a child with characteristics of Noonan syndrome[14]. However, we re-analyzed this case using oligo aCGH (including 21 probes that cover *MLL2*) and found the distal breakpoint to be located ~700 kb proximal to *MLL2* (data not shown). Also, all of the pathogenic missense variants identified here are located in regions of *MLL2* that encode C-terminal domains. This suggests that missense variants elsewhere in *MLL2* may be better tolerated or, alternatively, may be embryonically lethal.

For the 18 of 53 cases for which no previously unidentified protein-altering variant was found, it is possible that noncoding or other missed mutations in *MLL2* are responsible for this disorder. Alternatively, Kabuki syndrome could be genetically heterogeneous, and further analysis of these cases by exome sequencing may elucidate additional genes for Kabuki syndrome and potentially explain some of the phenotypic heterogeneity seen in this disorder. Notably, 9 of 10 individuals in the discovery cohort (90%), but only 26 of 43 individuals in the replication cohort (60%), were ultimately found to have mutations in *MLL2*. It is therefore possible that the careful selection of canonical Kabuki cases for the discovery cohort enriched for a shared genetic basis. This underscores the importance of access to deeply phenotyped and well-characterized cases.

In summary, we applied exome sequencing of a small number of unrelated individuals with Kabuki syndrome to discover that mutations in *MLL2* underlie this disorder. As predicted in previous analyses[2,3], allowing for even a small degree of genetic heterogeneity or missing data substantially confounds exome analysis by increasing the number of candidate genes consistent with the model of inheritance. To facilitate the prioritization of genes under such criteria, we stratified data by ranked phenotypes and found that *MLL2* was prominent in the higher ranked cases. However, nine of the ten individuals with Kabuki syndrome in the discovery cohort were ultimately found to have *MLL2* mutations, such that stratification by phenotype was of less importance than originally appeared to have been the case. Nonetheless, the sequential analysis of ranked cases may have reduced the probability of confounding due to genetic heterogeneity. All of the *MLL2* mutations found in the discovery set via exome sequencing were loss-of-function variants. As a result, *MLL2* ranked highly among candidate genes assessed by predicted functional impact. Such a pattern will likely occur for some, but not all, Mendelian phenotypes subjected to this approach. We anticipate that the further development of strategies to stratify data at both the genotypic and phenotypic level will be critical for exome and whole-genome sequencing to reach their full potential as tools for discovery of genes underlying Mendelian and complex diseases.

URLs. RefSeq 36.3, ftp://ftp.ncbi.nlm.nih.gov/genomes/MapView/Homo_sapiens/sequence/BUILD.36.3/updates/seq_gene.md.gz; Phaster, http://www.phrap.org; SeattleSeq Annotation, http://gvs.gs.washington.edu/SeattleSeqAnnotation/; 1000 Genomes Project, http://www.1000genomes.org/page.php/; dbGaP accession, http://www.ncbi.nlm.nih.gov/projects/gap/cgi-bin/study.cgi?study_id=phs000295.v1.p1.

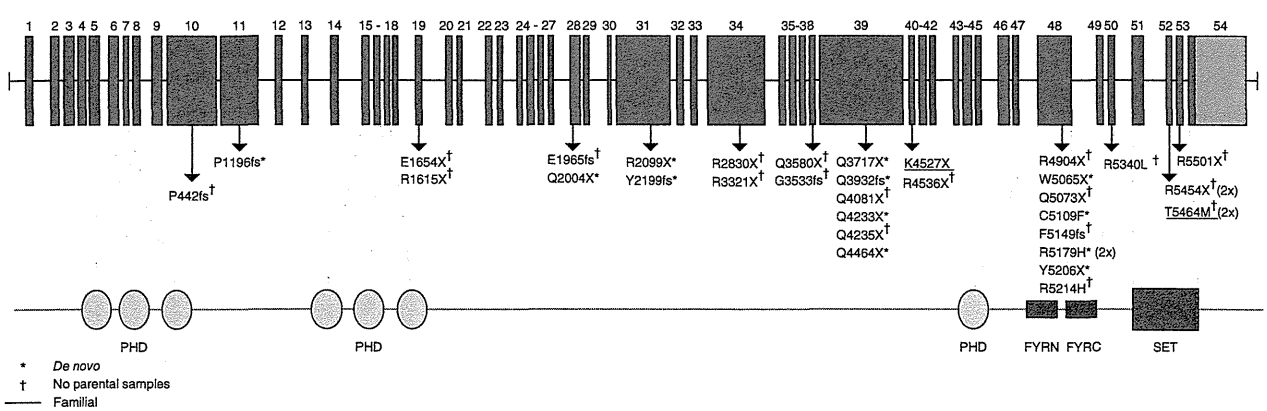

Figure 1 Genomic structure and allelic spectrum of *MLL2* mutations that cause Kabuki syndrome. *MLL2* is composed of 54 exons that encode untranslated regions (orange) and protein coding sequence (blue) including 7 PHD fingers (yellow), FYRN (green), FYRC (green) and a SET domain (red). Arrows indicate the locations of 32 different mutations found in 53 families with Kabuki syndrome including 20 nonsense mutations, 7 indels and 5 amino acid substitutions. Asterisks indicate mutations that were confirmed to be *de novo* and crosses indicate cases for which parental DNA was unavailable. The two underlined mutations were transmitted each within a family, from an affected parent to an affected child.

METHODS

Methods and any associated references are available in the online version of the paper at http://www.nature.com/naturegenetics/.

Accession codes. Exome data for the discovery cohort is available via the NCBI dbGaP repository under accession number phs000295.v1.p1.

Note: Supplementary information is available on the Nature Genetics website.

ACKNOWLEDGMENTS

We thank the families for their participation and the Kabuki Syndrome Network for their support. We thank J. Allanson, J. Carey and M. Golabi for referral of cases and M. Emond for helpful discussion. We thank the 1000 Genomes Project for early data release that proved useful for filtering out common variants. Our work was supported in part by grants from the US National Institutes of Health (NIH)–National Heart, Lung, and Blood Institute (5R01HL094976 to D.A.N. and J.S.), the NIH–National Human Genome Research Institute (5R21HG004749 to J.S., 1RC2HG005608 to M.J.B., D.A.N. and J.S.; and 5RO1HG004316 to H.K.T.), NIH–National Institute of Environmental Health Sciences (HHSN273200800010C to D.N. and M.J.R.), Ministry of Health, Labour and Welfare (K.Y., N.M., T.O. and N.N.), Japan Science and Technology Agency (N.M.), Society for the Promotion of Science (N.M.), the Life Sciences Discovery Fund (2065508 and 0905001), the Washington Research Foundation and the NIH–National Institute of Child Health and Human Development (1R01HD048895 to M.J.B.). S.B.N. is supported by the Agency for Science, Technology and Research, Singapore. A.W.B. is supported by a training fellowship from the NIH–National Human Genome Research Institute (T32HG00035).

AUTHOR CONTRIBUTIONS

The project was conceived and the experiments were planned by M.J.B., D.A.N. and J.S. The review of phenotypes and the sample collection were performed by M.J.B., M.C.H., M.J.M., K.Y., N.M., T.O. and N.N. Experiments were performed by S.B.N., K.J.B., A.E.B., C.L., H.C.M., J.D.S., M.J.R., E.H.T. and H.I.G. Ethical consultation was provided by H.K.T. Data analysis was performed by A.W.B., M.J.B., K.J.B., G.M.C., S.B.N. and J.S. The manuscript was written by M.J.B., S.B.N. and J.S. All aspects of the study were supervised by M.J.B. and J.S.

COMPETING FINANCIAL INTERESTS

The authors declare no competing financial interests.

Published online at http://www.nature.com/naturegenetics/.
Reprints and permissions information is available online at http://npg.nature.com/reprintsandpermissions/.

1. Choi, M. *et al.* Genetic diagnosis by whole exome capture and massively parallel DNA sequencing. *Proc. Natl. Acad. Sci. USA* **106**, 19096–19101 (2009).
2. Ng, S.B. *et al.* Exome sequencing identifies the cause of a Mendelian disorder. *Nat. Genet.* **42**, 30–35 (2010).
3. Ng, S.B. *et al.* Targeted capture and massively parallel sequencing of 12 human exomes. *Nature* **461**, 272–276 (2009).
4. FitzGerald, K.T. & Diaz, M.O. MLL2: A new mammalian member of the *trx/MLL* family of genes. *Genomics* **59**, 187–192 (1999).
5. Niikawa, N., Matsuura, N., Fukushima, Y., Ohsawa, T. & Kajii, T. Kabuki make-up syndrome: a syndrome of mental retardation, unusual facies, large and protruding ears, and postnatal growth deficiency. *J. Pediatr.* **99**, 565–569 (1981).
6. Kuroki, Y., Suzuki, Y., Chyo, H., Hata, A. & Matsui, I. A new malformation syndrome of long palpebral fissures, large ears, depressed nasal tip, and skeletal anomalies associated with postnatal dwarfism and mental retardation. *J. Pediatr.* **99**, 570–573 (1981).
7. Niikawa, N. *et al.* Kabuki make-up (Niikawa-Kuroki) syndrome: a study of 62 patients. *Am. J. Med. Genet.* **31**, 565–589 (1988).
8. Courtens, W., Rassart, A., Stene, J.J. & Vamos, E. Further evidence for autosomal dominant inheritance and ectodermal abnormalities in Kabuki syndrome. *Am. J. Med. Genet.* **93**, 244–249 (2000).
9. Cooper, G.M. *et al.* Distribution and intensity of constraint in mammalian genomic sequence. *Genome Res.* **15**, 901–913 (2005).
10. Cooper, G.M. *et al.* Single-nucleotide evolutionary constraint scores highlight disease-causing mutations. *Nat. Methods* **7**, 250–251 (2010).
11. Prasad, R. *et al.* Structure and expression pattern of human *ALR*, a novel gene with strong homology to *ALL-1* involved in acute leukemia and to *Drosophila* trithorax. *Oncogene* **15**, 549–560 (1997).
12. Issaeva, I. *et al.* Knockdown of ALR (MLL2) reveals ALR target genes and leads to alterations in cell adhesion and growth. *Mol. Cell. Biol.* **27**, 1889–1903 (2007).
13. Glaser, S. *et al.* Multiple epigenetic maintenance factors implicated by the loss of Mll2 in mouse development. *Development* **133**, 1423–1432 (2006).
14. Tonoki, H., Saitoh, S. & Kobayashi, K. Patient with del(12)(q12q13.12) manifesting abnormalities compatible with Noonan syndrome. *Am. J. Med. Genet.* **75**, 416–418 (1998).

ONLINE METHODS

Cases and samples. For exome sequencing, we selected ten individuals of self-reported European, Hispanic or mixed European and Haitian ancestry with Kabuki syndrome from ten unrelated families. Phenotypic data were collected from review of medical records, phone interviews and photographs. All participants provided written consent, and the Institutional Review Boards of Seattle Children's Hospital and the University of Washington approved all studies. The clinical characteristics of the 43 individuals in the validation cohort who had been diagnosed with Kabuki syndrome have been reported previously[7]. Subjective assessment and ranking of the Kabuki phenotype was based on pictures of each subject (**Supplementary Fig. 1**) and clinical information (**Supplementary Table 1**). Informed consent was obtained for publication of each of the facial photos shown.

Exome definition, array design and target masking. We targeted all protein-coding regions as defined by RefSeq 36.3. Entries were filtered for the following: (i) CDS as the feature type, (ii) transcript name starting with "NM_" or "-", (iii) reference as the group_label, (iv) not being on an unplaced contig (for example, 17|NT_113931.1). Overlapping coordinates were collapsed for a total of 31,922,798 bases over 186,040 discontiguous regions. A single custom array (Agilent, 1M features, aCGH format) was designed to have probes over these coordinates as previously described[3], except here, the maximum melting temperature (T_m) was raised to 73 °C.

The mappable exome was also determined as previously described[3] using this RefSeq exome definition instead. After masking for 'unmappable' regions, 30,923,460 bases were left as the mappable target.

Targeted capture and massive parallel sequencing. Genomic DNA was extracted from peripheral blood lymphocytes using standard protocols. Five micrograms of DNA from each of ten individuals with Kabuki syndrome was used for construction of a shotgun sequencing library as described previously[3] using paired-end adaptors for sequencing on an Illumina Genome Analyzer II (GAII). Each shotgun library was hybridized to an array for target enrichment; this was then followed by washing, elution and additional amplification. Enriched libraries were then sequenced on a GAII to get either single-end or paired-end reads.

Read mapping and variant analysis. Reads were mapped and processed largely as previously described[3]. In brief, reads were quality recalibrated using Eland and then aligned to the reference human genome (hg18) using Maq. When reads with the same start site and orientation were filtered, paired-end reads were treated like separate single-end reads; this method is overly conservative and hence the actual coverage of the exomes is higher than reported here. Sequence calls were performed using Maq and these calls were filtered to coordinates with ≥8× coverage and consensus quality ≥ 20.

Indels affecting coding sequences were identified as previously described[3], but we used phaster instead of cross_match and Maq. Specifically, unmapped reads from Maq were aligned to the reference sequence using phaster (version 1.100122a) with the parameters -max_ins:21 -max_del:21 -gapextend_ins:-1 -gapextend_del:-1 -match_report_type:1. Reads were then filtered for those with at most two substitutions and one indel. Reads that mapped to the negative strand were reverse complemented and, together with the other filtered reads, were remapped using the same parameters to reduce ambiguity in the called indel positions. These reads were then filtered for (i) having a single indel more than 3 bp from the ends and (ii) having no other substitutions in the read. Putative indels were then called per individual if they were supported by at least two filtered reads that started from different positions. An 'indel reference' was generated as previously described[3], and all the reads from each individual were mapped back to this reference using phaster with default settings and -match_report_type:1. Indel genotypes were called as previously described[3].

To determine the novelty of the variants, sequence calls were compared against 16 individuals for whom we had previously reported exome data[2,3] and 10 EGP exomes. Annotations of variants were based on NCBI and UCSC databases using an in-house server (SeattleSeqAnnotation). Loss-of-function variants were defined as nonsense mutations (premature stop) or frame-shifting indels. For each variant, we also generated constraint scores as implemented in GERP[10].

***Post hoc* ranking of candidate genes.** Candidate genes were ranked by summation of a case score and variant score. The case score was calculated by counting the total number of Kabuki exomes in which a variant was identified at a given gene, weighted for case rank from 1 to 10. For example, the top ranked case was weighted by a factor of 10, whereas the case ranked tenth was weighted by a factor of 1. The variant score was calculated by first counting the total number of nonsense, nonsynonymous and synonymous variants across the ten Kabuki exomes and assigning a prior probability of the occurrence of each variant type per gene based upon the target of 18,918 genes. Next, for each candidate gene shared among two or more Kabuki exomes, the scores for each newly identified variant were summed across the gene. The case score and variant score were summed as the candidate gene score.

Mutation validation. Sanger sequencing of PCR amplicons from genomic DNA was used to confirm the presence and identity of variants in the candidate gene identified via exome sequencing and to screen the candidate gene in additional individuals with Kabuki syndrome.

Array comparative genomic hybridization (CGH). Samples were hybridized to commercially available whole-genome tiling arrays consisting of one million oligonucleotide probes with an average spacing of 2.6 kb throughout the genome (SurePrint G3 Human CGH Microarray 1x1M, Agilent Technologies). Twenty-one probes on this array covered *MLL2* specifically. Data were analyzed using Genomics Workbench software according to the manufacturer's instructions.

ARTICLE

SMOC1 Is Essential for Ocular and Limb Development in Humans and Mice

Ippei Okada,[1,14] Haruka Hamanoue,[1,2,14] Koji Terada,[3] Takaya Tohma,[4] Andre Megarbane,[5] Eliane Chouery,[5] Joelle Abou-Ghoch,[5] Nadine Jalkh,[5] Ozgur Cogulu,[6] Ferda Ozkinay,[6] Kyoji Horie,[7] Junji Takeda,[7,8] Tatsuya Furuichi,[9,10] Shiro Ikegawa,[9] Kiyomi Nishiyama,[1] Satoko Miyatake,[1] Akira Nishimura,[1] Takeshi Mizuguchi,[1,15] Norio Niikawa,[11,12] Fumiki Hirahara,[2] Tadashi Kaname,[13] Koh-ichiro Yoshiura,[12] Yoshinori Tsurusaki,[1] Hiroshi Doi,[1] Noriko Miyake,[1] Takahisa Furukawa,[3] Naomichi Matsumoto,[1,*] and Hirotomo Saitsu[1,*]

Microphthalmia with limb anomalies (MLA) is a rare autosomal-recessive disorder, presenting with anophthalmia or microphthalmia and hand and/or foot malformation. We mapped the MLA locus to 14q24 and successfully identified three homozygous (one nonsense and two splice site) mutations in the SPARC (secreted protein acidic and rich in cysteine)-related modular calcium binding 1 (*SMOC1*) in three families. *Smoc1* is expressed in the developing optic stalk, ventral optic cup, and limbs of mouse embryos. *Smoc1* null mice recapitulated MLA phenotypes, including aplasia or hypoplasia of optic nerves, hypoplastic fibula and bowed tibia, and syndactyly in limbs. A thinned and irregular ganglion cell layer and atrophy of the anteroventral part of the retina were also observed. Soft tissue syndactyly, resulting from inhibited apoptosis, was related to disturbed expression of genes involved in BMP signaling in the interdigital mesenchyme. Our findings indicate that SMOC1/Smoc1 is essential for ocular and limb development in both humans and mice.

Introduction

Microphthalmia with limb anomalies (MLA [MIM 206920]), also known as Waardenburg anophthalmia syndrome or ophthalmoacromelic syndrome, is a rare autosomal-recessive disorder first described by Waardenburg.[1] It is characterized by ocular anomalies ranging from mild microphthalmia to true anophthalmia and by limb anomalies such as oligodactyly, syndactyly, and synostosis of the 4th and 5th metacarpals.[2–4] The genetic cause for MLA has remained unknown.

It is widely known that secreted signaling molecules such as Sonic hedgehog (Shh), wingless-type MMTV integration site family (Wnt), transforming growth factor β (Tgf-β), bone morphogenetic proteins (Bmps), and fibroblast growth factor (Fgf) are involved in the development of many organs and tissues, including the eyes and limbs.[5,6] In particular, mutations in *BMP4* (MIM 112262) have resulted in anophthalmia with systemic manifestations, including polydactyly and/or syndactyly (also known as micropthalmia, syndromic 6, MCOPS6 [MIM 607932]),[7] highlighting importance of BMP signaling in both the developing eye and limb.

SMOC1 (MIM 608488), which encodes SPARC (secreted protein acidic and rich in cysteine)-related modular calcium binding 1, is a member of the SPARC (also known as BM-40) matricellular protein family that modulates cell-matrix interaction by binding to many cell-surface receptors, the extracellular matrix, growth factors, and cytokines.[8,9] SMOCs are extracellular glycoproteins with five domains: an N-terminal follistatin-like (FS) domain, two thyroglobulin-like (TY) domains, a domain unique to SMOC, and an extracellular calcium-binding (EC) domain.[9] SMOC1 is widely expressed in various tissues with localization to basement membranes.[9,10] Although the biological function of SMOC1 remains largely unknown, it has been recently reported that *Xenopus* smoc protein, the ortholog of human SMOC1, acts as a BMP antagonist,[11] suggesting that human SMOC1 can also modulate BMP signaling.

Here, we demonstrate that *SMOC1* mutations cause MLA. We also show that *Smoc1* null mice recapitulated

[1]Department of Human Genetics, Yokohama City University Graduate School of Medicine, 3-9 Fukuura, Kanazawa-ku, Yokohama 236-0004, Japan; [2]Department of Obstetrics and Gynecology, Yokohama City University Graduate School of Medicine, 3-9 Fukuura, Kanazawa-ku, Yokohama 236-0004, Japan; [3]Department of Developmental Biology, Osaka Bioscience Institute, 6-2-4 Furuedai, Suita, Osaka 565-0874, Japan; [4]Division of Pediatrics, Okinawa Prefectural Nanbu Medical Center & Children's Medical Center, 118-1 Ikyoku, Arakawa, Haebaru, Okinawa 901-1193, Japan; [5]Medical Genetics Unit, St. Joseph University, Beirut 1104-2020, Lebanon; [6]Department of Pediatrics, Ege University Faculty of Medicine, 35100 Bornova-Izmir, Turkey; [7]Department of Social and Environmental Medicine, Graduate School of Medicine, Osaka University, 2-2 Yamadaoka, Suita, Osaka 565-0871, Japan; [8]Center for Advanced Science and Innovation, Osaka University, 2-1 Yamadaoka, Suita, Osaka 565-0871, Japan; [9]Laboratory for Bone and Joint Disease, Center for Genomic Medicine, RIKEN, 4-6-1 Shirokanedai, Minato-ku, Tokyo 108-8639, Japan; [10]Laboratory Animal Facility, Research Center for Medical Sciences, Jikei University School of Medicine, 3-25-8, Nishi-Shimbashi, Minato-ku, Tokyo 105-8461, Japan; [11]Research Institute of Personalized Health Sciences, Health Sciences University of Hokkaido, Ishikari-Tobetsu, Hokkaido 061-0293, Japan; [12]Department of Human Genetics, Nagasaki University Graduate School of Biomedical Sciences, Sakamoto 1-12-4, Nagasaki 852-8523, Japan; [13]Department of Medical Genetics, University of the Ryukyus Faculty of Medicine, 207 Uehara, Nishihara, Okinawa 903-0215, Japan
[14]These authors contributed equally to this work
[15]Current address: Laboratory of Biochemistry and Molecular Biology, National Cancer Institute, National Institutes of Health, Building 37, Room 6050, Bethesda, MD 20892, USA
*Correspondence: naomat@yokohama-cu.ac.jp (N.M.), hsaitsu@yokohama-cu.ac.jp (H.S.)
DOI 10.1016/j.ajhg.2010.11.012.

MLA phenotypes, indicating that *SMOC1* plays essential roles in both eye and limb development in humans and mice.

Subjects and Methods

Subjects

A total of four families with one or two cases of MLA were analyzed in this study, including three previously reported families (A, B, and C).[12,13] Family X from Turkey, which has been previously described,[14] was newly recruited to this study. Detailed clinical information of all the patients is available in the literature,[12,14] and phenotypes of patients with confirmed mutations are summarized in Table S1 (available online). A total of five affected and 16 unaffected members from the four families were analyzed in the linkage study. Genomic DNA was obtained from peripheral-blood leukocytes with the use of QuickGene 610-L (Fujifilm, Tokyo, Japan) after informed consent had been given. Experimental protocols were approved by the institutional review board of Yokohama City University School of Medicine.

SNP Genotyping, and Fine Mapping with Short Tandem Repeat Markers

Whole-genome SNP genotyping, with the use of GeneChip Human Mapping 50K Array XbaI (Affymetrix, Santa Clara, CA), and fine mapping of possible candidate regions, with the use of additional microsatellite markers, were performed as previously described.[12,15] The list of primers used for fine mapping is presented in Table S2.

Linkage Analysis

Multipoint linkage analyses using aligned SNPs were performed with ALLEGRO software.[16] Two-point linkage analyses of candidate regions were performed with the LINKAGE package MLINK (FASTLINK software, version 5.1). In each program, an autosomal-recessive model of inheritance with complete penetrance and a disease-allele frequency of 0.001 were applied.

Mutation Analysis of Candidate Genes

All coding exons and exon-intron boundaries of *RAD51L1* (MIM 602948), *ACTN1* (MIM 102575), *ERH* (MIM 601191), *SRSF5* (MIM 600914), *DCAF5* (MIM 603812), *COX16*, *EXD2*, *GALNTL1*, *SLC39A9*, *KIAA0247*, *MED6* (MIM 602984), *TTC9* (MIM 610488), *MAP3K9* (MIM 600136), and *SMOC1* (transcript variant 1, GenBank accession number NM_001034852.1) were analyzed in the probands of families A, C, and X. The transcript variant 2 of *SMOC1* (GenBank accession number NM_022137.4) is 3 bp shorter than the variant 1, leading to an in-frame amino acid deletion at position 431. PCR was cycled 35 times at 94°C for 30 s, at 60°C for 30 s, and at 72°C for 30–90 s in a total volume of 20 μl containing 30 ng genomic DNA as a template, 0.5 μM forward and reverse primers, 200 μM each deoxyribonucleotide triphosphate (dNTP), 1 × ExTaq buffer, and 0.25 U ExTaq (Takara). All primers were designed with Primer3 software. Detailed information of primers is available upon request. PCR products were purified with ExoSAP (USB) and sequenced with BigDye Terminator 3.1 (Applied Biosystems) on a 3100 Genetic Analyzer. Sequences of patients were compared to reference genome sequences in the UCSC Genome Browser (February 2009 assembly) with Seqscape software, version 2.1 (Applied Biosystems).

Animals

Smoc1 mutant mice, created with the use of the *Sleeping Beauty* transposon system, have been previously described.[17] Line PV384 was provided by the RIKEN BioResource Center through the National BioResource Project of MEXT, Japan. Three independent mouse lines (no. 1 to no. 3), each with a single insertion in intron 1 of *Smoc1*, were bred as heterozygotes. Lines 1 and 3 were backcrossed for at least four generations to a C57BL/6J background. Line 2 was maintained with a mixed background of C57BL/6J and ICR. We mainly analyzed line 1, but we confirmed similar phenotypes in lines 2 and 3. Animals were housed in accordance with protocols approved by the Institutional Animal Care and Use Committee at Yokohama City University, School of Medicine. PCR genotyping of mice was performed with the use of genomic DNA from yolk-sac, ear, or tail biopsies. The following primers were used: PV384-WF, 5′-AAAGGCTGGGAATTGTTTG A-3′; PV384-WR, 5′-TGCAGCTGAAACTGTCTCTCC-3′; PV384-MF, 5′-TGTCCTAACTGACTTGCCAAA-3′. The PV384-WF/PV384-WR primers amplified a 441 bp wild-type (WT) product, and the PV384-MF/PV384-WR primers amplified a 218 bp mutant product.

Southern Hybridization

Genomic DNA was extracted from livers or tail biopsies of PV384 heterozygous (*Smoc1*$^{Tp/+}$) mice via standard protocols. The gene-trap insertions were analyzed by Southern hybridization with the use of 10 μg of *Sac*I-, *Nde*I-, BglII-, and *Eco*RI-digested DNA. The probe (451 bp), which hybridized to the internal ribosome entry site (IRES) in the gene-trap vector, was synthesized with the DIG PCR Probe Synthesis Kit (Roche) with the use of the following primers: 5′-CTAACGTTACTGGCCGAAGC-3′ and 5′-CCCAGATCAGATCCCATACAA-3′. Hybridization, washing, and detection of probes were performed according to the manufacturer's protocol. Images were captured with the FluorChem system (Alpha Innotech).

Cloning of Gene-Trap Insertion Sites

After identification of aberrant DNA fragments by Southern hybridization, *Nde*I-, *Sac*I-, and *Eco*RI-digested DNA from PV384 mice was fractionated by electrophoresis, and appropriately sized fragments containing *Ol1* (*other locus 1*), *Ol2*, and *Ol3* were isolated with a QIAEXII Gel Extraction Kit (QIAGEN). The isolated DNA was self-ligated by Ligation High ver.2 (Toyobo), precipitated with ethanol, and dissolved in 20 μl EB buffer (QIAGEN). Inverse PCR was performed in 25 μl reactions, containing 2 μl ligated DNA, 1 × PCR buffer for KOD FX, 0.4 mM each dNTP, 0.5 μM each primer, and 0.5 U KOD FX DNA polymerase (Toyobo). Primers common to *Ol1*, *Ol2*, and *Ol3* were as follows: Inv-F, 5′- AT CGCCAGTTCTGTATGAACGGTCTGGTCTT-3′; Inv-R, 5′-CCCTC TTTACGTGCCAGCCATCTTAGAGATAC-3′. Confirmatory PCR of gene-trap insertion sites for *Ol1*, *Ol2*, and *Ol3* loci was performed with the use of the following primers: *Ol1*-F, 5′-GAGTGGTATTCA TTGGATTCTGCTGAT-3′; *Ol2*-F, 5′-AAATCCAGCTGGCCAACAGA CTAAG-3′; *Ol3*-F, 5′-TTGCCGGGTAGACTCTATCAAGAACCA-3′; TBAL-R, 5′-CTTGTGTCATGCACAAAGTAGATGTCC-3′. Primer sets of *Ol1*-F/TBAL-R, *Ol2*-F/TBAL-R, and *Ol3*-F/TBAL-R could amplify 175 bp, 607 bp, and 767 bp products, respectively. These PCR primer pairs were also used for genotyping of mice harboring a single insertion at the *Smoc1* locus.

Confirmation of Promoter- and Poly(A)-Trapped Transcripts

Whole embryos at embryonic day 10.5 (E10.5) and E11.5 were stored in RNAlater solution (QIAGEN). Total RNA was extracted from WT, *Smoc1*$^{Tp/+}$, and *Smoc1*$^{Tp/Tp}$ embryos with the use of RNeasy Plus Mini (QIAGEN). One microgram total RNA was subjected to reverse transcription with the use of a PrimeScript 1st Strand Synthesis Kit with random hexamers (Takara). A control reaction with no reverse transcriptase was included in each experiment. PCR was performed in 20 μl reactions, containing 1 μl cDNA, 1 × PCR Buffer for KOD FX, 0.4 mM each dNTP, 0.3 μM each primer, and 0.4 U KOD FX (Toyobo). Primers used are listed below: *Smoc1*-F, 5′-GTCCCCACCTCCCCAAGTGCTTTGA-3′; *LacZ*-R, 5′-TGCCAAAAGACGGCAATATGGTGGAAA-3′; *GFP*-F, 5′-TCACATGGTCCTGCTGGAGTTCGTGAC-3′; *Smoc1*-R, 5′-ACACTTGCTCTGGCCAGCATCTTTGCAT-3′. Primer sets of *Smoc1*-F/*Smoc1*-R, *Smoc1*-F/*LacZ*-R, and *GFP*-F/*Smoc1*-R could amplify native *Smoc1* (366 bp), promoter-trapped transcripts (Tp-LacZ, 500 bp) and poly(A)-trapped transcripts (Tp-GFP, 308 bp), respectively. The PCR conditions were 98°C for 10 s, 68°C for 1 min, for 30 cycles. Primers for *ACTB*[18] were used as an internal control. PCR for *ACTB* was cycled 20 times at 94°C for 20 s, 60°C for 20 s, and 72°C for 30 s in a total volume of 10 μl containing 0.5 μl cDNA, 0.4 μM each primer, 0.2 mM each dNTP, 1 × ExTaq buffer, and 0.5 U ExTaq HS (Takara). All PCR products were electrophoresed on 2% agarose gels.

In Situ Hybridization

Embryos were collected between E9.5 and E13.5. Whole-mount in situ hybridization was carried out as previously described.[19,20] Two fragments of *Smoc1* cDNA were obtained as probes by RT-PCR, with the use of total RNA extracted from livers of E16.5 mouse embryos, and subcloned into pCR4-TOPO (Invitrogen). Primer sequences were as follows: probe 1-F, 5′-GTCTGCTCACGCCCCACT-3′; probe 1-R, 5′-CCTGAACCATGTCTGTGGTG-3′; probe P-F, 5′-CAGGAACAGGAAAGGGAAGA-3′; probe P-R, 5′-AAGGGAAAACCACACAGCAC-3′. PCR products were 1023 bp and 1578 bp, corresponding to nucleotide positions 275–1297 and 1849–3426 of the mouse *Smoc1* cDNA (GenBank accession number NM_001146217.1), respectively. The cDNA fragment amplified with probe P-F and probe P-R primers was identical to the probe used in a previous report.[21] Digoxigenin-labeled sense and antisense riboprobes were synthesized with the use of a digoxigenin RNA labeling kit (Roche). These two different antisense probes demonstrated identical staining patterns, and the control sense probes showed no staining. The expression pattern was confirmed with more than three embryos. In addition, the following probes were used: *Bmp2* (gift from Y. Takahashi),[22] *Sox9* (gift from A. Yamada),[22] *Bmp7* (gift from E.J. Robertson), and *Msx2* (gift from Dr. R.E. Maxson, Jr). The numbers of embryos examined were as follows (numerical quantity for WT, *Smoc1*$^{Tp/+}$, and *Smoc1*$^{Tp/Tp}$, respectively, shown in parentheses): *Msx2* (2, 1, 3) at E11.5; *Bmp2* (3, 0, 3), *Bmp7* (3, 0, 3), *Msx2* (3, 0, 3), and *Sox9* (2, 1, 3) at E12.5; *Bmp2* (1, 2, 3), *Bmp7* (2, 1, 3), *Msx2* (1, 2, 3), and *Sox9* (1, 3, 4) at E13.5. Stained embryos were cleared in glycerol to enable images to be produced with a VHX-1000 digital microscope (Keyence).

Histology

Heads of embryos and newborns were fixed overnight in 4% paraformaldehyde in PBS at 4°C. These embryos were then washed in PBS. Frozen samples were serially sectioned at 16 μm (E14.5) and 20 μm (P0). The numbers of eyes examined (WT, *Smoc1*$^{Tp/+}$, *Smoc1*$^{Tp/Tp}$) were as follows: coronally sectioned at E14.5 (8, 10, 12), coronally sectioned at P0 (8, 10, 6), horizontally sectioned at P0 (2, 2, 4). For evaluation of ventral atrophy of the retina, only the coronally sectioned eyes were used. TB staining was performed according to standard protocols. Forelimbs of mice were fixed in 4% paraformaldehyde in PBS, decalcified in 10% EDTA, and embedded in paraffin. Forelimbs were serially sectioned at 4 μm and stained with hematoxylin and eosin.

Evaluation of Optic Nerve Diameter

The palatine and orbital bones were carefully removed to expose the optic chiasm and optic nerve. During the dissection process, 4% paraformaldehyde in PBS was frequently applied onto the gaps between the bone and optic nerve. Xylene cyanol was applied to enhance the outline of optic nerves at poastnatal day 0 (P0). Photographs of optic nerves were taken with a VHX-1000 digital microscope, and the diameter was measured for right and left optic nerves with the bundled software included with the VHX-1000 instrument.

Skeletal Staining

For skeletal preparations, mice were fixed in 99.5% ethanol after removal of the skin and viscera. Cartilage tissues were stained with 0.015% alcian blue and 20% acetic acid in 75% ethanol for three days at 37°C. After dehydration with 99.5% ethanol for three days, bones were stained with 0.002% alizarin red in 1% KOH. Then skeletons were cleared in 1% KOH for several weeks. For P14 mice, soft tissues were dissolved in 2% KOH before alizarin red staining.

Nile Blue Staining

For the study of apoptosis of hindlimbs at E13.5 and E14.5, Nile blue (NB) staining was performed on the basis of a previously described protocol,[23] except that staining was performed at 37°C (not room temperature). Apoptosis was determined by NB-stained (deceased) cells. After rinsing in Tyrode solution, hindlimbs of control (WT and heterozygous littermates) and homozygous mice were evaluated. Photographs of dorsal aspects were taken with a VHX-1000 digital microscope. Experiments were repeated three times, and reproducible representative results are presented.

Statistical Analysis

Statistical analyses were performed with the use of non-repeated-measures ANOVA followed by Dunnett's post hoc test. The results are given as mean ± standard deviation, and the threshold p value for statistical significance was 0.01.

Results

Identification of Homozygous *SMOC1* Mutations

We have previously mapped the MLA locus to a 422 kb region at 10p11.23 by analyzing three families (one Japanese family [A] and two Lebanese families [B and C]). This region contained only one gene, *MPP7*, in which no mutations were found.[12] After a new Turkish family (X) was added to the analysis, the MLA locus was again searched by homozygosity mapping to the consanguineous families (X, B, and C) and haplotype mapping to family A for detection of compound-heterozygous mutations; however, we could not detect any common regions

among the four families. We then focused on identifying common regions in any three of the four families to allow for locus heterogeneity (Table S3).

A locus at 14q24.1-q24.2, which showed the highest LOD score (3.936) among the candidate regions larger than 2.0 Mb, was highlighted among families A, C, and X. This locus was analyzed with the use of additional microsatellite markers, and a 3.0 Mb region containing 24 genes was identified (Figures 1A and 1B). A total of 14 genes were sequenced, and homozygous mutations were found in *SMOC1*: c.718C>T (p.Gln240X) in family A, c.664+1G>A in family C, and c.378+1G>A in family X (Figures 1C and 1D). All of these homozygous mutations were cosegregated with the disease phenotype, and the parents of the individuals with these mutations were heterozygous carriers (Figure 1C). We could not find any mutations in *SMOC1* in family B, in which MLA is unlinked to the 14q24.1-q24.2 locus. Interestingly, in family A haplotypes of paternal and maternal alleles, each having the same mutation, are completely different (data not shown), suggesting that the same mutation may have occurred in separate events. The c.718C>T mutation was not detected in 289 healthy Japanese controls, including 100 Okinawa islanders. The other two mutations were not detected in ethnically matched controls (54 Lebanese and 99 Turkish subjects, respectively), nor in 289 Japanese controls. The two splice-donor-site mutations (c.664+1G>A and c.378+1G>A) are predicted to abolish a donor site, as predicted by ESE-finder, NetGene2, HSF2.4.1, SpliceView, and BDGP analysis (Table S4). Thus, the three mutations are likely to lead to a loss of functional SMOC1.

Smoc1 Expression in the Developing Eye and Limb in Mice

For the examination of *Smoc1* expression in the developing eye and limb, whole-mount in situ hybridization of mouse embryos was performed. *Smoc1* was expressed in the forebrain, midbrain, hindbrain, pharyngeal arch, somites, and forelimb buds at E9.5 (Figure 2A). At E10.5, *Smoc1* expression was observed in the optic stalk (Figure 2B), and at E11.5, expression was localized to the closure site of the optic cup (Figure 2C). Expression of *Smoc1* in developing limbs between E10.5 and E11.5 was observed in both dorsal and ventral regions, with a broader pattern of expression in dorsal regions, but expression was not detected in the most anterior, posterior, and distal parts of limb buds (Figures 2D and 2E). Expression coinciding with chondrogenic condensation was observed at E12.5 (Figure 2F), and expression then became restricted to future synovial joint regions at E13.5 (Figure 2G). This dynamic expression suggests that *Smoc1* plays a critical role in ocular and limb development.

Ocular and Limb Anomalies in *Smoc1* Null Mice

To investigate the pathological basis of MLA due to the loss of *SMOC1* function, we obtained *Smoc1* mutant mice, PV384.[17] PV384 mice possess gene-trap insertions in the *Smoc1* locus and in three other loci. After PV384 mice were bred with C57BL/6J or ICR mice, we obtained three independent lines (no. 1 to no. 3), each with a sole insertion in intron 1 of *Smoc1* (Figure S1). We mainly analyzed line 1, but we confirmed similar phenotypes in lines 2 and 3. Heterozygous mutant mice ($Smoc1^{Tp/+}$) were healthy and fertile. Homozygous mice ($Smoc1^{TP/TP}$) were null mutants, as they showed no native transcript of *Smoc1* (Figure S1E). Homozygous mice were viable at P0; however, they did not survive beyond the first 3 wks of life (Figure 3B). Their growth was retarded in comparison to WT and heterozygous littermates at P0 and P14 (Figures 3A and 3C). Developmental defects in eyes and optic nerves were evident at E14.5. Homozygous mice had relatively small eyes, and histological examinations revealed aplasia or hypoplasia of optic nerves (in 10 of 12 optic nerves), atrophy of the anteroventral part of the retina (in 11 of 12 eyes), and extension of the retinal pigmented epithelium (RPE) to the optic nerve (in 10 of 12 eyes) (Figures 3D–3I). These abnormalities were also observed at P0 (aplasia or hypoplasia of optic nerves [in 7 of 10 optic nerves], retinal atrophy [in 6 of 6 eyes], and RPE extension [in 3 of 6 eyes with identifiable optic nerves]) (Figures 3J–3M). WT or heterozygous littermates did not show any such abnormalities, except that a few eyes of heterozygous mice showed extension of the RPE at E14.5, but not at P0 (in 2 of 10 and 0 of 12 eyes, respectively). Toluidine blue (TB) staining showed ganglion cell layers that were thinned and irregular to varying degrees in homozygous mice, suggesting a reduced number of retinal ganglion cells (Figures 3J–3K'). Thus, *Smoc1* is required for axon sprouting, elongation, or maintenance of retinal ganglion cells.[24] Hypoplasia of optic nerves was further quantitatively confirmed by macroscopic examination: the average diameter of optic nerves of homozygous mice was significantly smaller than that of WT and heterozygous littermates at P0 and P14 (Figures 3L–3Q). These data clearly demonstrate that loss of *Smoc1* in mice affects development of the body, retina, and optic nerves, in a manner similar to that seen in MLA patients.[3,4]

Newborn homozygous mice could be readily identified by their hindlimb syndactyly and pes valgus, whereas no abnormalities were observed in WT and heterozygous pups (Figure 4 and Table 1). Interestingly, the severity of syndactyly varied between mouse lines: line 1 exclusively showed soft tissue syndactyly, whereas line 2 frequently showed four digits (Figures 4F and 4J). Skeletal preparations with alcian blue and alizarin red revealed that the foot with four digits had four phalanx and five metatarsals with fusion to each other (Figure 4K). Thus the *Smoc1* null mutation resulted in a spectrum of phenotypes, from soft tissue syndactyly to four fused digits, probably due to different genetic backgrounds. Bowed tibiae and hypoplastic fibulae were also consistently observed in homozygous mice (Figures 4H and 4L). The articulation between

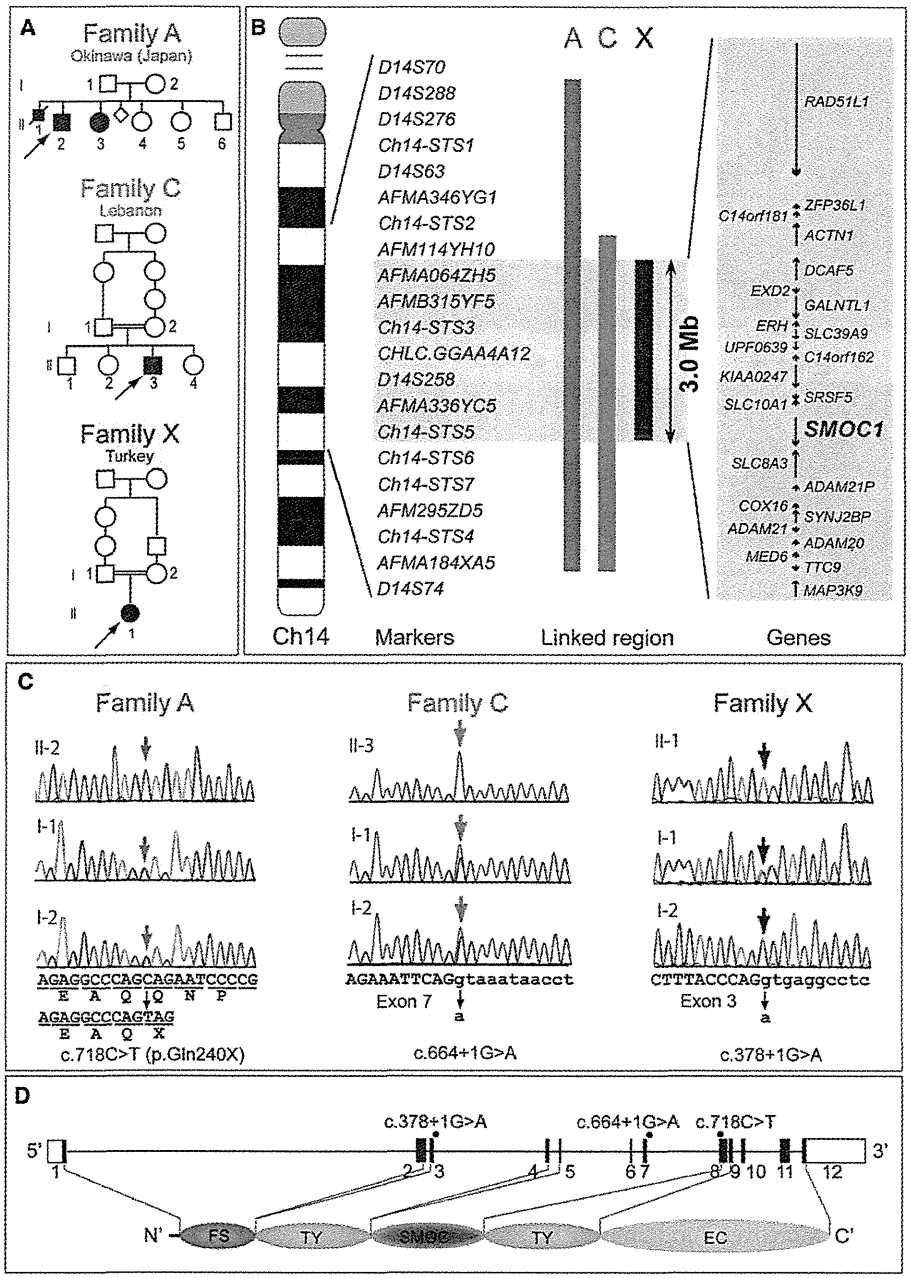

Figure 1. Genetic Analysis of Three Families with Members Affected by Microphthalmia with Limb Anomalies
(A) Pedigrees of the three families.
(B) Linkage analysis with SNPs and microsatellite markers on chromosome 14. From left to right: chromosome ideogram, genetic markers, linked regions of the three families, and genes mapped to the shortest overlapping linked region (between *AFM114YH10* and *Ch14-STS6* [UCSC coordinates, Feb. 2009: chromosome 14: 68,388,190–71,347,908 bp]).
(C) Sequences of mutations identified in each family. Affected patients in family A have a homozygous nonsense mutation (c.718C>T). Patients in families C and X have distinct homozygous splice-donor site mutations (c.664+1G>A and c.378+1G>A, respectively). For all mutations, parents of affected patients are heterozygous carriers, without exception. Sequences of the exon and intron are presented in upper and lower cases, respectively.
(D) At the top is a depiction of a schematic representation of *SMOC1* consisting of 12 exons (UTR and coding exons are indicated by open and filled rectangles, respectively). The locations of three mutations are indicated by red dots. At the bottom, the functional domains of SMOC1 are depicted. Abbreviations are as follows: FS, the follistatin-like domain; TY, the thyroglobulin-like domain; SMOC, the domain unique to SMOC; and EC, the extracellular calcium-binding domain.

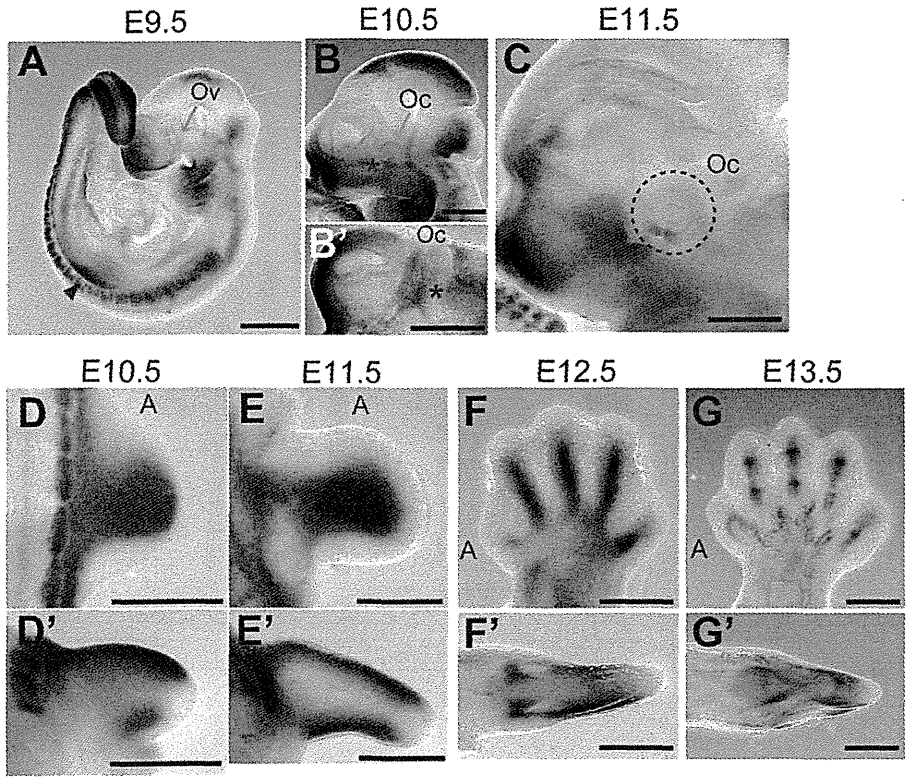

Figure 2. *Smoc1* Expression in Mouse Embryos
Lateral views of embryos (A–C) and a ventral view of the left part of the head (B′, lateral view is shown at the top).
(A) At E9.5, *Smoc1* was expressed in the forebrain, midbrain, hindbrain, pharyngeal arch, somites, and forelimb buds (magenta arrowhead), but not in the optic vesicle (Ov, blue arrow).
(B and B′) Expression in the optic stalk became evident at E10.5 (magenta asterisks), but was not evident in the optic cup (Oc, blue arrow).
(C) Expression was restricted to the closure site of the optic cup (dashed circle) at E11.5.
(D–G) Dorsal and (D′–G′) posterior view of the right hindlimbs (dorsal view is shown at the top in D′–G′). The anterior side is indicated by an A. (D and D′) At E10.5, *Smoc1* was more widely expressed in the dorsal part of the limb bud than in the ventral part. *Smoc1* expression is undetected in the most anterior, posterior, and distal parts of the limb bud. (E and E′) At E11.5, ventral expression was broader than that in the previous stage. (F and F′) At E12.5, expression was detected in areas consistent with chondrogenic condensation. (G and G′) At E13.5, *Smoc1* expression became restricted to future joint regions. Scale bar represents 500 μm.

tibia/fibula and calcanea of homozygous mice appeared malpositioned (Figures 4G and 4K), which might contribute to pes valgus. At P14, soft tissue syndactyly was also evident in most forelimbs of homozygous mice (Figures 4M–4O). Moreover, hindlimbs of homozygous mice showed synostosis between the 4th and 5th metatarsals (Figure 4T), which is observed in both the hands and the feet of MLA patients. Thus, many limb anomalies of MLA patients were recapitulated in *Smoc1* null mice (Table S1).

Reduced Interdigital Apoptosis and Disturbed BMP Signaling

Among the various abnormalities caused by loss of *Smoc1* function, we focused on soft tissue syndactyly, which was commonly observed in both fore- and hindlimbs of null mutants. It is possible that the syndactyly is caused by failed apoptotic regression of the interdigital mesenchyme. To examine this hypothesis, hindlimbs were stained with NB sulfate at E13.5 and E14.5, the time when interdigital apoptosis is most evident. In control embryos (WT and heterozygous littermates), NB-stained apoptotic cells were identified in the interdigital mesenchyme, where regression of the interdigital webbing occurs in the distal region (Figures 5A and 5C). By contrast, the number of apoptotic cells in the mesenchyme between digits 2 and 3 and digits 3 and 4 was dramatically reduced in homozygous mice at E13.5 and E14.5, along with persistent webbing in the distal region (Figures 5B and 5D, magenta asterisk). BMP signaling is involved in apoptosis of the interdigital mesenchyme.[25,26] *Bmp2*, *Bmp7*, and *Msx2*, a direct target of BMP signaling, were strongly expressed in the interdigital mesenchyme of control hindlimbs at both E12.5 and E13.5. However, the expression of these three genes was profoundly reduced and perturbed in hindlimbs of homozygous mice (Figures 5E–5J). These data suggest that inhibition of apoptosis is spatiotemporally correlated to reduced and/or disturbed expression of genes involved in BMP signaling in the interdigital mesenchyme.

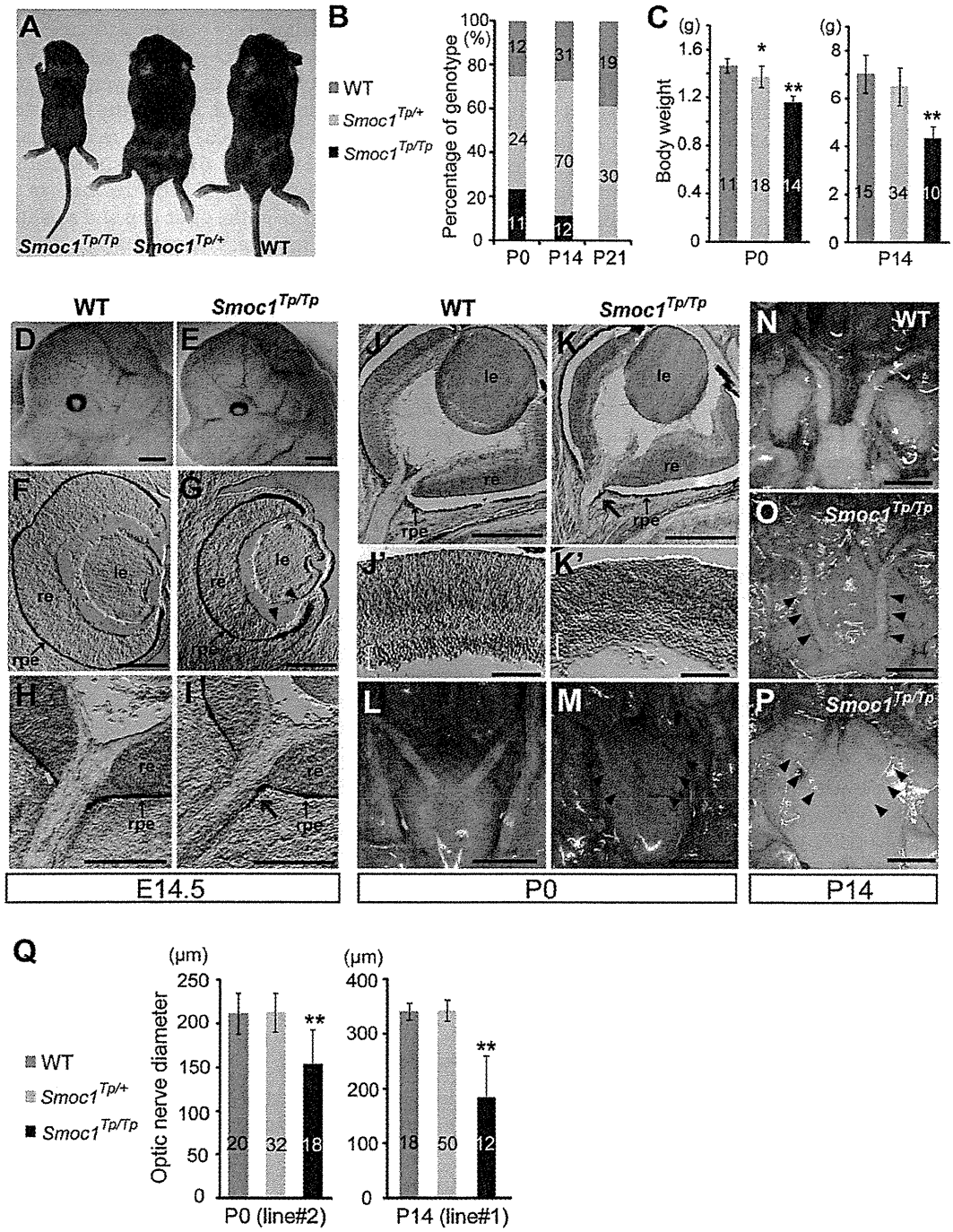

Figure 3. Growth and Ocular Phenotypes of *Smoc1* Null Mice

(A) Representative *Smoc1*$^{Tp/Tp}$ mouse, showing a small body in comparison to *Smoc1*$^{Tp/+}$ and WT littermates.

(B) Genotypes of living pups during the first 3 wk of life.

(C) Body weight of pups of each genotype at P0 (left panel) and P14 (right panel).

(D and E) Relatively small eyes were evident in *Smoc1*$^{Tp/Tp}$ mice in comparison to WT mice.

(F–K′) Coronal sections of eyes at E14.5 (F–I) and P0 (J–K′) with TB staining (H, I, and J–K′). (F-I) Atrophy of the anteroventral part of the retina (G, magenta arrowheads, dorsal view shown at the top), hypoplastic optic nerve, and extension of the RPE to the optic nerve (I, magenta arrow) in *Smoc1*$^{Tp/Tp}$ mice at E14.5. (J and K) Hypoplastic optic nerve and RPE extension in *Smoc1*$^{Tp/Tp}$ mice at P0 (K, magenta arrow). Note that sections in which optic nerves appeared most thick are presented in (H–K). (J′–K′) In higher-magnification views of (J and K), a thinned and irregular ganglion cell layer (white brackets) was observed in *Smoc1*$^{Tp/Tp}$ mice. Abbreviations are as follows: le, lens; re, retina; rpe, retinal pigmented epithelium.

(L–P) Ventral views of the brain showing optic nerves at P0 (L and M) and P14 (N–P), showing various degrees of optic nerve hypoplasia.

Discussion

In a previous report, we performed parametric linkage analysis with three families (families A, B, and C) and found 16 loci showing a LOD score ($\theta = 0.000$) higher than 3.0. Additional microsatellite markers highlighted only one locus, 10p11.23.[12] However, no mutations were found in the candidate gene *MPP7*.[12] By recruiting a new family (family X) to this study, we successfully found homozygous mutations in *SMOC1* in families A, C, and X. In family B, no *SMOC1* mutations were found, indicating the genetic heterogeneity in MLA. Patients with *SMOC1* mutations and *Smoc1* null mice showed similar limb anomalies, such as oligodactyly, syndactyly, synostosis of 4th and 5th metacarpals, hypoplasia of fibula, and bowed tibia. Oligodactyly, syndactyly, and synostosis of 4th and 5th metacarpals are common in MLA patients.[2–4] However, hypoplastic fibula and bowed tibia are less common in patients with MLA, as four out of 34 MLA patients showed these anomalies in the previous report.[3] Although one patient with a *SMOC1* mutation from family C did not show bowed tibia and hypoplastic fibula, these anomalies could be features specific to *SMOC1* mutations. Further *SMOC1* analysis of other MLA patients should delineate the phenotypic consequences caused by *SMOC1* mutations.

Accumulating evidence suggests that BMP signaling plays crucial roles in early eye vesicle and limb patterning, skeletal formation, and apoptosis of the interdigital mesenchyme,[25–29] and mutations involving BMP signaling cause human malformations including ocular, limb, and skeletal anomalies.[7,30–33] Here, we present genetic evidence that *SMOC1* is essential for ocular and limb development in humans and mice. Furthermore, *Xenopus smoc* can inhibit BMP signaling,[11] suggesting that *SMOC1/Smoc1* can also modulate BMP signaling in humans and mice. Indeed, we observed reduced and/or disturbed expression of genes involved in BMP signaling in the interdigital mesenchyme in *Smoc1* null mice, and limb and ocular abnormalities associated with loss of *Smoc1* function are consistent with phenotypic consequences of disturbed BMP signaling. Conditional inactivation of *Bmp2* in the limb showed 3/4 syndactyly, and a similar deficiency of both *Bmp2* and *Bmp7* resulted in malformed fibulae in mice.[25] Moreover, mice deficient in *Fmn1*, a repressor of BMP signaling, showed four digits, fused metatarsal bones, and an absence of fibulae in the hindlimbs,[34] suggesting the importance of altered BMP signaling in these features. Concerning ocular phenotypes, haploinsufficiency of mouse *Bmp4* resulted in a decreased number of ganglion layer cells and absence of the optic nerve similar to *Smoc1* null mice,[35] indicating that altered BMP signaling is also involved in the ocular phenotype. Interestingly, knockdown experiments of *smoc* by antisense morpholino in *Xenopus* showed absence or severe deformity of the eye and other anterior structures, which were accompanied by aberrant expression of *otx2*, *tbx2* in the eye field.[11] Mutations of *OTX2* (MIM 600037) cause micropthalmia, syndromic 5 (MCOPS5 [MIM 610125]) in humans.[36] Moreover, targeted disruption of *Tbx2* resulted in a marked reduction in the size of the optic cup and a failure of optic nerve formation in mice.[37] Thus, it is possible that loss of *SMOC1* function could alter the expression of *OTX2* and *TBX2* (MIM 600747) by disturbing BMP signaling in human developing eyes.

It is unknown how the loss of functional SMOC1, a BMP antagonist, leads to reduced expression of genes involved in BMP signaling in the interdigital mesenchyme in *Smoc1* null mice. In the case of *Fmn1*-deficient mice, the loss of the repressor of BMP signaling resulted in downregulation of *Fgf4* and *Shh* and in upregulation of *Gremlin* expression at E10.5, and absence of apoptosis of the interdigital mesenchyme between the two middle digits at E13.5.[34] Thus, there is a possibility that loss of SMOC1 could cause the imbalance among BMP, SHH, and FGF signaling, which would subsequently lead to reduced and/or disturbed expression of genes involved in BMP signaling in the interdigital mesenchyme. In fact, we observed reduced expression of *Msx2* in the progressive zone of hindlimbs at E11.5 (Figure S2). Moreover, expression of *Sox9*, the initial cartilage condensation marker, showed abnormal limb patterning, suggesting that SMOC1 may affect BMP signaling even at early stages of limb development (Figure S3). Further examinations are required for understanding spatial and temporal actions of SMOC1/Smoc1 protein during limb development.

In conclusion, our data demonstrate that *SMOC1/Smoc1* is an essential player in both ocular and limb development in humans and mice and give further support to the crucial roles of BMP signaling in these systems.

Supplemental Data

Supplemental Data include three figures and four tables and can be found with this article online at http://www.cell.com/AJHG/.

Acknowledgments

We would like to thank the patients and their families for their participation in this study. We thank Yoshiko Takahashi (Nara Institute of Science and Technology) and Atsushi Yamada (Showa University) for providing the *Bmp2* and *Sox9* probes; Elizabeth J. Robertson (University of Oxford) and Makoto Ishibashi (Kyoto University) for the *Bmp7* probe; Robert E. Maxson, Jr. (University of Southern California Keck School of Medicine) for the *Msx2*

(Q) Optic nerve diameter. Optic nerves were significantly hypoplastic in $Smoc1^{Tp/Tp}$ mice in comparison to WT and $Smoc1^{Tp/+}$ littermates. The numbers of pups (B and C) or eyes (Q) corresponding to each genotype are indicated within bars. Error bars indicate standard deviation: *$p < 0.01$, compared with WT. **$p < 0.01$, compared with WT and $Smoc1^{Tp/+}$. Scale bars represent 1 mm (D, E, and L–P), 200 μm (F–I), 500 μm (J and K), and 100 μm (J′ and K′).

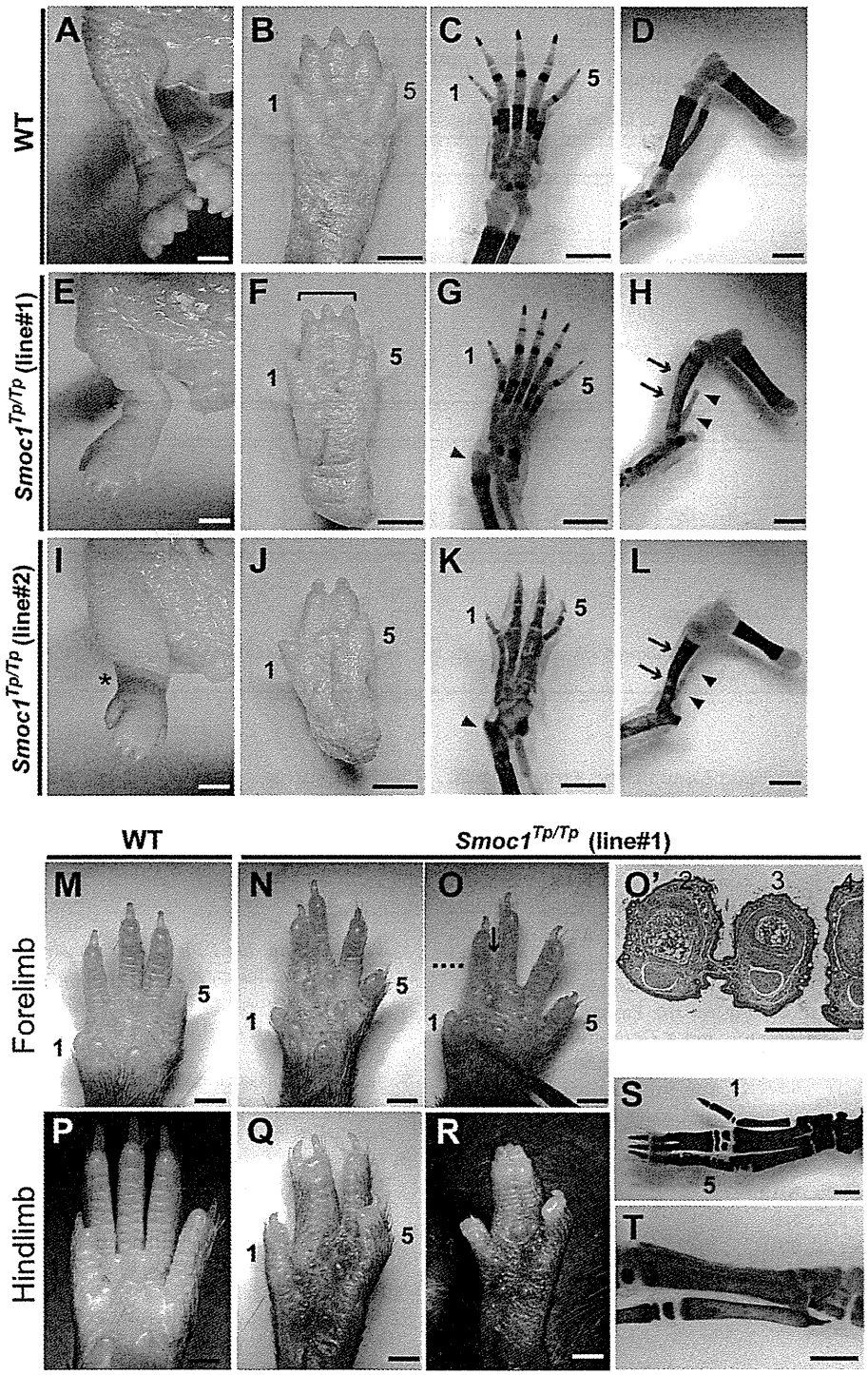

Figure 4. Limb Phenotypes of *Smoc1* Null Mice

Limbs of WT (A–D, M, and P) and *Smoc1*$^{Tp/Tp}$ mice (E–L, N–O′, and Q–T) at P0 (A–L) and P14 (M–T). Digit identities are indicated by the numbers 1 (thumb, anterior) and 5 (little finger, posterior). Skeletal staining with alcian blue and alizarin red is presented (C, D, G, H, K, L, S, and T). *Smoc1*$^{Tp/Tp}$ mice showed pes valgus (E and I), soft tissue syndactyly (F and G), and four digits with metatarsal fusion (J and K). Malposition of the articulation between the tibia/fibula and the calcanea (G and K, magenta arrowheads), bowed tibia (magenta arrows), and hypoplastic fibula (arrowheads) of *Smoc1*$^{Tp/Tp}$ mice (H and L) were observed. 2/3 soft tissue syndactyly (N) and 2/3 webbing (O) were evident in forelimbs of *Smoc1*$^{Tp/Tp}$ mice. (O′) A transverse section taken at the level indicated by the dashed line in (O) showed 2/3 webbing. 2/3 syndactyly (Q), 2/3/4 syndactyly (R), synostosis between the 2nd and 3rd proximal phalanx and metatarsals (S), and synostosis between the 4th and 5th metatarsals (T, arrow), observed in the hindlimbs of *Smoc1*$^{Tp/Tp}$ mice. Scale bars represent 1 mm (A–O and P–T) or 500 μm (O′).

Table 1. Limb Abnormalities in *Smoc1*$^{Tp/Tp}$ Mutants

Genotype	Talipes Valgus (No. of Affected/ Total No. of Pups)	Forelimb Abnormalities (No. of Limbs)	Hindlimb Syndactyly (No. of Limbs)					Other External Abnormalities (No. of Pups)	4th and 5th Metatarsal Fusion (No. of Affected/Total No. of Limbs)
			None	2/3[a]	3/4[b]	2/3/4[c]	4 Digits		
Postnatal Day 0									
Smoc1$^{Tp/+}$ (line 1, C57BL/6J)	0/42	0	84	0	0	0	0		
Smoc1$^{Tp/+}$ (line 2, ICR mixed)	0/38	0	76	0	0	0	0		
Smoc1$^{Tp/Tp}$ (line 1, C57BL/6J)	10/10	0	3	0	3	12	2		
Smoc1$^{Tp/Tp}$ (line 2, ICR mixed)	13/17	1[d]	1	1	9	4	19	cleft palate (3)	
Postnatal Day 14									
Smoc1$^{Tp/+}$ (line 1, C57BL/6J)	0/70	0	140	0	0	0	0		
Smoc1$^{Tp/Tp}$ (line 1, C57BL/6J)	11/11	18[e]	2	7	3	8	2	hypoplastic thumbs (5)	9/10[f]

[a] Syndactyly between the 2nd and 3rd digits.
[b] Syndactyly between the 3rd and 4th digits.
[c] Syndactyly between the 2nd, 3rd, and 4th digits.
[d] 2/3 soft tissue syndactyly.
[e] Eleven limbs showed 2/3 webbing, four limbs showed 2/3 soft tissue syndactyly, and one limb showed 3/4 syndactyly.
[f] Based on examination of skeletal preparations.

probe; Tomonori Hirose, Kazunori Akimoto, and Kazunori Sasaki (Yokohama City University) for providing useful information about mouse breeding, taking photos on a stereo microscope, and mRNA quantification; and Kohei Shiota and Sumiko Kimura (Kyoto University) for helpful comments about NB staining and limb anomalies. This work was supported by research grants from the Ministry of Health, Labour and Welfare (T. Furuichi, N. Miyake, N. Matsumoto, and H.S.) and the Japan Science and Technology Agency (N. Matsumoto), a Grant-in-Aid for Scientific Research from the Japan Society for the Promotion of Science (T. Furuichi and N. Matsumoto), and a Grant-in-Aid for Young Scientist from the Japan Society for the Promotion of Science (K.N., H.D., N. Miyake, and H.S.). This work has been carried out at the Advanced Medical Research Center of Yokohama City University.

Received: September 29, 2010
Revised: November 20, 2010
Accepted: November 26, 2010
Published online: December 30, 2010

Web Resources

The URLs for data presented herein are as follows:

BDGP, http://www.fruitfly.org/
ESEfinder 3.0, http://rulai.cshl.edu/cgi-bin/tools/ESE3/esefinder.cgi?process=home
GenBank, http://www.ncbi.nlm.nih.gov/Genbank/
HSF2.4.1, http://www.umd.be/HSF/
NetGene2, http://www.cbs.dtu.dk/services/NetGene2/
Online Mendelian Inheritance in Man, http://www.ncbi.nlm.nih.gov/Omim
UCSC Genome Browser, http://genome.ucsc.edu/cgi-bin/hgGateway
SpliceView, http://zeus2.itb.cnr.it/~webgene/wwwspliceview.html

References

1. Waardenburg, P.J. (1961). Autosomally-recessive anophthalmia with malformations of the hands and feet. In Genetics and Ophthalmology, P.J. Waardenburg, A. Franceschetti, and D. Klein, eds. (Assen, The Netherlands: Royal Van Gorcum), p. 773.
2. Teiber, M.L., Garrido, J.A., and Barreiro, C.Z. (2007). Ophthalmo-acromelic syndrome: report of a case with vertebral anomalies. Am. J. Med. Genet. A. *143A*, 2460–2462.
3. Garavelli, L., Pedori, S., Dal Zotto, R., Franchi, F., Marinelli, M., Croci, G.F., Bellato, S., Ammenti, A., Virdis, R., Banchini, G., and Superti-Furga, A. (2006). Anophthalmos with limb anomalies (Waardenburg opththalmo-acromelic syndrome): report of a new Italian case with renal anomaly and review. Genet. Couns. *17*, 449–455.
4. Tekin, M., Tutar, E., Arsan, S., Atay, G., and Bodurtha, J. (2000). Ophthalmo-acromelic syndrome: report and review. Am. J. Med. Genet. *90*, 150–154.
5. Adler, R., and Canto-Soler, M.V. (2007). Molecular mechanisms of optic vesicle development: complexities, ambiguities and controversies. Dev. Biol. *305*, 1–13.
6. Zeller, R., López-Ríos, J., and Zuniga, A. (2009). Vertebrate limb bud development: moving towards integrative analysis of organogenesis. Nat. Rev. Genet. *10*, 845–858.
7. Bakrania, P., Efthymiou, M., Klein, J.C., Salt, A., Bunyan, D.J., Wyatt, A., Ponting, C.P., Martin, A., Williams, S., Lindley, V., et al. (2008). Mutations in BMP4 cause eye, brain, and digit

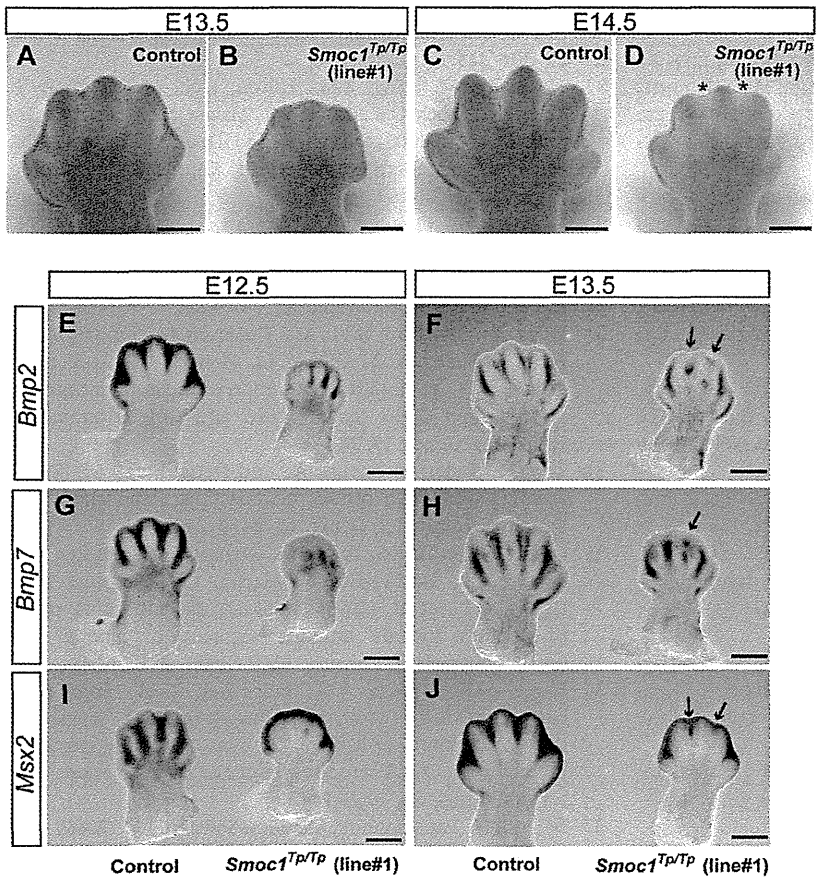

Figure 5. Reduced Apoptosis and Altered BMP Signaling in the Interdigital Mesenchyme of *Smoc1* Null Mice

(A–D) NB staining of left hindlimbs at E13.5 (A and B) and E14.5 (C and D). In comparison to control embryos (WT and $Smoc1^{Tp/+}$ littermates) (A and C), the number of NB-stained apoptotic cells in the interdigital mesenchyme of $Smoc1^{Tp/Tp}$ mice was dramatically reduced between digits 2 and 3 and digits 3 and 4 at both E13.5 and E14.5, and the webbing remained at a distal level (B and D, magenta asterisk).

(E–J) Whole-mount in situ hybridization of right hindlimbs at E12.5 (E, G, and I) and E13.5 (F, H, and J). At E12.5, interdigital expression of *Bmp2*, *Bmp7*, and *Msx2* was profoundly delayed in the hindlimbs of $Smoc1^{Tp/Tp}$ mice, and their expression in the interdigital mesenchyme was apparently perturbed, even at E13.5 (magenta arrows). Scale bar represents 500 μm.

developmental anomalies: overlap between the BMP4 and hedgehog signaling pathways. Am. J. Hum. Genet. *82*, 304–319.

8. Bornstein, P., and Sage, E.H. (2002). Matricellular proteins: extracellular modulators of cell function. Curr. Opin. Cell Biol. *14*, 608–616.
9. Vannahme, C., Smyth, N., Miosge, N., Gösling, S., Frie, C., Paulsson, M., Maurer, P., and Hartmann, U. (2002). Characterization of SMOC-1, a novel modular calcium-binding protein in basement membranes. J. Biol. Chem. *277*, 37977–37986.
10. Gersdorff, N., Müller, M., Schall, A., and Miosge, N. (2006). Secreted modular calcium-binding protein-1 localization during mouse embryogenesis. Histochem. Cell Biol. *126*, 705–712.
11. Thomas, J.T., Canelos, P., Luyten, F.P., and Moos, M., Jr. (2009). Xenopus SMOC-1 inhibits BMP signaling downstream of receptor binding and is essential for post-gastrulation development in Xenopus. J. Biol. Chem. *284*, 18994–19005.
12. Hamanoue, H., Megarbane, A., Tohma, T., Nishimura, A., Mizuguchi, T., Saitsu, H., Sakai, H., Miura, S., Toda, T., Miyake, N., et al. (2009). A locus for ophthalmo-acromelic syndrome mapped to 10p11.23. Am. J. Med. Genet. A. *149A*, 336–342.
13. Mégarbané, A., Souraty, N., and Tamraz, J. (1998). Ophthalmo-acromelic syndrome (Waardenburg) with split hand and polydactyly. Genet. Couns. *9*, 195–199.
14. Cogulu, O., Ozkinay, F., Gündüz, C., Sapmaz, G., and Ozkinay, C. (2000). Waardenburg anophthalmia syndrome: report and review. Am. J. Med. Genet. *90*, 173–174.
15. Miyake, N., Kosho, T., Mizumoto, S., Furuichi, T., Hatamochi, A., Nagashima, Y., Arai, E., Takahashi, K., Kawamura, R., Wakui, K., et al. (2010). Loss-of-function mutations of CHST14 in a new type of Ehlers-Danlos syndrome. Hum. Mutat. *31*, 966–974.
16. Gudbjartsson, D.F., Thorvaldsson, T., Kong, A., Gunnarsson, G., and Ingolfsdottir, A. (2005). Allegro version 2. Nat. Genet. *37*, 1015–1016.
17. Keng, V.W., Yae, K., Hayakawa, T., Mizuno, S., Uno, Y., Yusa, K., Kokubu, C., Kinoshita, T., Akagi, K., Jenkins, N.A., et al. (2005). Region-specific saturation germline mutagenesis in mice using the Sleeping Beauty transposon system. Nat. Methods *2*, 763–769.
18. Mamo, S., Gal, A.B., Bodo, S., and Dinnyes, A. (2007). Quantitative evaluation and selection of reference genes in mouse oocytes and embryos cultured in vivo and in vitro. BMC Dev. Biol. *7*, 14.
19. Parr, B.A., Shea, M.J., Vassileva, G., and McMahon, A.P. (1993). Mouse Wnt genes exhibit discrete domains of expression in the early embryonic CNS and limb buds. Development *119*, 247–261.
20. Saitsu, H., Ishibashi, M., Nakano, H., and Shiota, K. (2003). Spatial and temporal expression of folate-binding protein 1 (Fbp1) is closely associated with anterior neural tube closure in mice. Dev. Dyn. *226*, 112–117.
21. Tamplin, O.J., Kinzel, D., Cox, B.J., Bell, C.E., Rossant, J., and Lickert, H. (2008). Microarray analysis of Foxa2 mutant mouse embryos reveals novel gene expression and inductive roles